ILLINOIS CENTER FOR TRANSPORTATION

Chip Seal Quality Assurance Using Percent Embedment

Prepared By
Ahmad Alhasan
Brian Moon
Doug Steele
Hyung Lee
Abu Ahmed Sufian

Applied Research Associates, Inc.

Research Report No. FHWA-ICT-23-022

A report of the findings of

ICT PROJECT R27-221
Chip Seal Quality Assurance Using Percent Embedment

Illinois Center for Transportation

December 2023

TECHNICAL REPORT DOCUMENTATION PAGE

1. Report No. FHWA-ICT-23-022	2. Government Accession No. N/A	3. Recipient's Catalog No. N/A
4. Title and Subtitle Chip Seal Quality Assurance Using Percent Embedment		5. Report Date December 2023
		6. Performing Organization Code N/A
7. Authors Ahmad Alhasan, https://orcid.org/0000-0002-0091-9899, Brian Moon, Doug Steele, Hyung S. Lee, https://orcid.org/0000-0003-1616-7449, and Abu Ahmed Sufian		8. Performing Organization Report No. ICT-23-029 UILU-2023-2029
9. Performing Organization Name and Address Illinois Center for Transportation Department of Civil and Environmental Engineering University of Illinois at Urbana-Champaign 205 North Mathews Avenue, MC-250 Urbana, IL 61801		10. Work Unit No. N/A
		11. Contract or Grant No. R27-221
12. Sponsoring Agency Name and Address Illinois Department of Transportation (SPR) Bureau of Research 126 East Ash Street Springfield, IL 62704		13. Type of Report and Period Covered Final Report 8/16/20–12/31/23
		14. Sponsoring Agency Code

16. Abstract

This study investigates the use of macrotexture as an indicator of the percent embedment (PE) of aggregate in a chip seal and ultimately, as a quality assurance tool for chip seals. The study included an extensive field- and controlled-testing program from 24 chip seal sections constructed in Illinois. Surface texture measurements were acquired using a high-speed texture profiler and a stationary laser texture device. The analysis showed that stationary texture measurements were more consistent and reliable for estimating PE and characterizing chip seals in the field. Moreover, the ground truth PE values were estimated using an image analysis algorithm implemented on side-view images of cores extracted in the field. The ground truth PE values were estimated using four approaches: the average elevation method, percent embedment of each aggregate method, the peak method, and the aggregate circumference method. The analysis showed that the correlations between the different PE estimation methods are relatively weak, indicating the various methods provide different information and may relate to different characteristics. The general regression models for PE values estimated using the average elevation method and the mean profile depth (MPD) acquired using laser texture scans and the average least dimension (ALD) yielded the highest R^2 value of 0.50. The model showed a consistent decreasing trend between PE and MPD estimated using laser texture scans and side-view images. Moreover, the model matched the expected behavior that PE should reach 100% as MPD reaches 0. Finally, four models were recommended correlating PE estimated using the average elevation and each aggregate methods to the MPD (mm) estimated from laser texture scans and ALD (mm) estimated from side-view images.

17. Key Words Chip Seal, Percent Embedment, Quality Assurance, Macrotexture, Laser Texture Scanning, Image Analysis	18. Distribution Statement No restrictions. This document is available through the National Technical Information Service, Springfield, VA 22161.		
19. Security Classif. (of this report) Unclassified	20. Security Classif. (of this page) Unclassified	21. No. of Pages 64 + appendices	22. Price N/A

Form DOT F 1700.7 (8-72)   **Reproduction of completed page authorized**

ACKNOWLEDGMENT, DISCLAIMER, MANUFACTURERS' NAMES

EXECUTIVE SUMMARY

Chip seal application is a common practice for maintenance and preservation of pavements. Chip seal application is used mainly to seal fine cracks on a pavement surface and to prevent water intrusion into the pavement foundation, thereby extending the life span of the existing pavement. In addition, chip seals are frequently used to restore surface texture and friction in an effort to improve some skid-resistant characteristics and to improve roadway safety.

Although quality assurance (QA) is important for all paving and treatment projects, there is no agreement on a well-established quantitative procedure and QA program for chip seal practice in the literature. State highway agencies may have different procedures for simplified QA measurements of chip seals. One of the practices is to estimate the percent embedment (PE) by pulling some of the chips after construction and visually examining the PE values. This practice does not guarantee representative samples and lacks consistency and objectivity because there are no specifications on how to measure PE from retrieved aggregates. The macrotexture of a chip seal surface may provide a close relationship to the PE of aggregates. As such, several studies have proposed using macrotexture as an indicator of the percent embedment and, subsequently, as a QA tool for chip seals. However, the effectiveness of these macrotexture measurements for QA of chip seals is not well established, especially under field conditions.

To investigate the relationship between surface texture and PE, two testing phases were performed in 2021 and 2022. The field-testing program in 2021 included 10 in-service chip seal sections in Illinois. In 2022, a construction project on a road segment along Illinois Route 116 near Roseville included nine unique test sections with varying materials and construction methods. In addition to the construction project sections, five in-service sections were tested to further validate the test procedures. Combining the sites tested in 2021 and 2022, the study included 24 test sections. The test sites covered a wide range of treatment ages and locations to capture different traffic volumes, materials used in these locations, and construction practices such as binder and chip application rates.

At each site, tests were performed within a 152 m (500 ft) test section marked using reflective tape at the beginning and end of the section. The field tests included high-speed texture profiles acquired on the left and right wheel paths. Three repetitions of the high-speed texture profiles were acquired at 56 kmh (35 mph) for each site. Following the high-speed texture profiles, handheld stationary laser texture scans were acquired at 15, 76, and 137 m (50, 250, and 450 ft) measured from the beginning of the test sections. Finally, cores were extracted for the handheld scanning locations in the right wheel path for additional texture scans, cross section image acquisition, and overhead image analysis.

Based on the evaluation performed in this study, the stationary laser texture scanner provided more consistent and reliable texture measurements and showed significant correlation to the estimated PE values. It is recommended to acquire a minimum of one stationary texture measurement every 60 m (~200 ft) in the field, with a minimum of three texture scans for each construction site. Additional texture scans may be required if high variability is observed in the test section. At each texture scan

location, it is recommended to acquire a minimum of 100 scan lines for a scan width of 71.61 × 101.60 mm (2.82 × 4.00 in.). The recommended maximum point spacing in each line is 7.94 × 10^{-3} mm (3.13 × 10^{-3} in.). Moreover, the analysis showed that mean profile depth (MPD) provided sufficient information for estimating PE values. In addition, power spectral density (PSD) provided more detailed information that can be used to compare different laser texture measurement devices and tools.

The acquired cores were trimmed, and images were acquired from the four sides of the trimmed cores to estimate the ground truth PE values using in-house image-analysis algorithms. In addition to estimating PE values, the side-view images were used to estimate surface texture and the average least dimension (ALD) of the aggregates. The ground truth PE values were estimated using four approaches: (1) the average elevation method, (2) percent embedment of each aggregate method, (3) the peak method, and (4) the aggregate circumference method. The analysis showed that the correlations between the different PE estimation methods are relatively weak, indicating the methods provide different information and may relate to different characteristics.

To investigate the relationship between PE and surface texture measurements, simple linear and multiple linear regression models were developed using the PE values estimated using various methods and texture parameters. With five texture parameters, including wavelet energies, and four PE estimation methods, the total number of possible basic models correlating PE to texture characteristics is 20. Additional models can be derived when separating the two test phases and incorporating ALD as a model parameter. Out of 80 possible combinations, the most reliable models correlated the PE estimated when using each aggregate and average elevation methods with MPD calculated using the laser texture scanner and side-view images.

In summary, regression models for PE values estimated using the average elevation method were consistent for Phase I and Phase II data. The models showed a consistent decreasing trend between PE and MPD estimated using the laser texture scans and side-view images. Moreover, the models for PE estimated using the average elevation method matched the expected behavior that PE should reach 100% as MPD reaches 0. This physical interpretability is very important when selecting the appropriate empirical models and definitions.

In addition to the simple linear models, two possible multiple linear regression models were evaluated. The first set of multiple linear regression models were developed by adding ALD in addition to MPD as a regression variable. The second set of multiple linear regression models included ALD and the interaction between MPD and ALD as a third regression variable. Adding the estimated ALD as a model variable significantly improved the model's performance and predictive power. Similar to the conclusions from the simple linear regression models, the models derived for PE estimated using the average elevation method outperformed the models developed for PE estimated using the average of PE values measured for each aggregate. Moreover, the models including MPD and ALD as the regression variables were always selected over the models including the interaction variable.

To derive a general regression model, data from Phases I and II were combined and analyzed. In addition, PE values, ALD, and MPD estimated from the side-view images were averaged for each core.

This represents more realistic results, because it averages the results from all sides of the same core. The general regression models for PE values estimated using the average elevation method and the MPD acquired using laser texture scans yielded the highest R^2 value. The next most reliable general regression models are the ones for PE values estimated using the each aggregate method and the MPD acquired using laser texture scans. The models showed a consistent decreasing trend between PE and MPD estimated using laser texture scans and side-view images. Accordingly, four models were recommended correlating PE estimated using the average elevation method and each aggregate method to the MPD (mm) estimated from laser texture scans and ALD (mm) estimated from side-view images.

Finally, to overcome the need for coring in the field, a prototype frame was designed and built to acquire laser texture scans and overhead images of chip seal surfaces in the field or in a controlled environment using cores. An analysis procedure and algorithms were developed to process the acquired overhead texture scans and images. This procedure estimates the exposed aggregate heights accurately and then estimates the PE values assuming the ALD of these aggregates. The estimation of the exposed aggregates is consistent and accurate; however, the estimated PE will require more accurate ALD measurements and will be mostly applicable for chip seals constructed with a single aggregate size.

TABLE OF CONTENTS

LIST OF FIGURES

LIST OF TABLES

CHAPTER 1: INTRODUCTION

BACKGROUND

Chip seal applications are a common maintenance and preservation treatment for pavements. These applications are used mainly to seal fine cracks on a pavement surface and to prevent water intrusion into the pavement foundation, thereby extending the life of the existing pavement. In addition, chip seals are used to improve surface skid-resistant characteristics, thereby improving roadway safety (Gransberg & James 2005).

In general, chip seal applications involve applying a layer of asphalt binder or emulsion followed by a layer of aggregate (chips). These chips are embedded and reoriented in the binder by passing a roller over the newly spread aggregate layer. The performance of chip seals depends on percent embedment, which is defined as the ratio between the height of the asphalt binder (i.e., the depth of aggregate embedment) and the height of the aggregate. The target embedment should be within a controlled range, typically between 70% after placement to 50% during service life. Higher embedment can lead to higher bleeding/flushing potential, while lower embedment can lead to aggregate loss and raveling (Mcleod et al., 1969). Figure 1 shows an idealized cross-section of a chip seal surface for illustration.
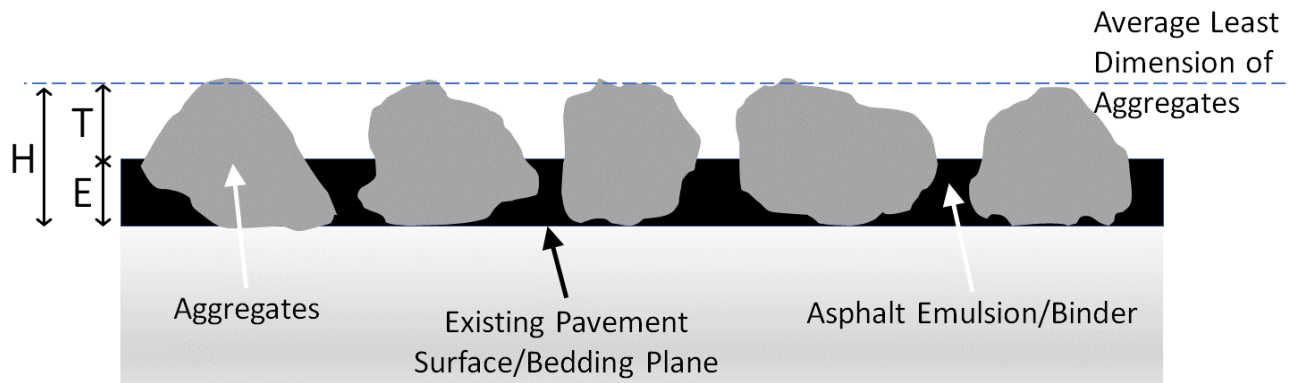
Figure 1. Sketch. Idealized chip seal cross-section.

As illustrated in Figure 1, the percent embedment (PE) can be obtained as follows:

$$PE = E/H = (H - T)/H$$

Figure 2. Equation. Estimation of percent embedment from texture for idealized chip seal profile.

Source: Shuler et al. (2011).

where *T* is the macrotexture depth of the chip seal surface, *E* is the height of the binder, and *H* is the height of the aggregate.

Recent studies have shown that a close link or correlation may exist between the surface macrotexture (T) and percent embedment (PE) of chip seals (Kutay & Ozdemir, 2016). However, typical texture measurements, including mean profile depth (MPD) or mean texture depth (MTD), may not provide all necessary parameters needed for calculating the percent embedment according to the equation in Figure 2. These measurements only provide an estimate of T, without any insight into E or H). Furthermore, texture measurements alone do not capture the effect of aggregate penetration into the substrate as well as the aggregate size distribution or orientation (Boz et al., 2019).

RESEARCH OBJECTIVES

The macrotexture of a chip seal surface may be related to the percent embedment of aggregates. As such, several studies have proposed to use macrotexture as an indicator of the percent embedment and, subsequently, as a quality assurance (QA) tool for chip seal construction. However, the effectiveness of these macrotexture measurements for QA of chip seals is not well established, especially under field conditions. Therefore, there is a need to evaluate the relationship between surface macrotexture and the percent embedment of chip seals under different field conditions.

In light of the above, the objectives of this study are listed as follows:

1. Determine if texture measurements can be used to calculate the percent embedment accurately.

2. Identify the appropriate surface texture measurement as well as other parameters to be correlated with percent embedment.

3. Identify an accurate and cost-effective method for chip seal texture measurement using the best available technology.

REPORT ORGANIZATION

This report is composed of six chapters and three appendices. Chapter 1 provides brief background information and discusses the need for this research. Chapter 2 documents the literature review and the simple national survey of the state of the practice. Chapter 3 documents the data collection procedures in the field and the cores acquired for image analysis and ground truthing. The chapter discusses the procedures for texture measurements in the field and in a controlled environment, coring, side images, and overhead image acquisitions. Chapter 4 documents the analysis procedures and algorithms used for texture analysis and ground truthing of the PE values estimated using the side images for cross-sections from the acquired cores. In addition, the analysis included overlapping 3D texture scans and overhead images to estimate the exposed height (not embedded in emulsion/binder) of the top aggregate layers from chip seal cores. Chapter 5 presents a summary and discussion of the analysis findings performed in accordance with the procedures described in Chapter 4. The analysis results include the impact of different texture scanning procedures and requirements on the accuracy of surface texture characterization. The texture characteristics were then correlated to the ground truth PE values estimated using image analysis. In addition to the use of surface texture

analysis, this chapter outlines the results for measuring exposed surfaces and estimating the percent embedment of the aggregates using overhead images. Chapter 6 provides conclusions of this study along with practical recommendations for implementation and future research.

CHAPTER 2: LITERATURE REVIEW AND SURVEY

This chapter documents the findings from the literature review encompassing both national and international research studies related to current practices and proposed procedures for QA and performance prediction of chip seals using PE and texture measurments. This effort focused on gathering information related to (1) the possible impact of PE on chip seal distresses including raveling and bleeding, (2) the relationship between surface texture and performance of chip seals, and (3) the use of surface texture as an indicator of QA or PE estimates for chip seals.

QUALITY ASSURANCE OF CHIP SEALS

QA can be defined as planned and systematic actions taken by owners and contractors to provide the necessary confidence that the procured material and workmanship will satisfy the quality requirements of the contract (AASHTO R10). Steps in QA include quality control, acceptance, and independent assurance.

Although QA is important for all paving and treatment projects, there is no agreement on well-established quantitative procedures and QA programs for chip seal practices in the literature. State highway agencies have different procedures for simplified QA measurements of chip seals. One of the practices is to estimate PE by pulling some of the chips after construction and visually examining the PE values. This practice does not guarantee representative samples and lacks consistency and objectivity because there are no specifications on how to measure PE from retrieved aggregates.

The Federal Highway Administration (2017) developed a chip seal "checklist" for state and local highway preservation/maintenance crew and inspection staff on the use and maintenance of chip seals. Few studies have investigated the use of measured emulsion/binder and aggregate application rates, surface characteristics measurement, and controlled laboratory or field-fabricated sample characteristics as QA measurements for chip seals.

Chip Seal Performance and QA Measurements

Performance of chip seals is affected by multiple factors including, but not limited to, the quality of materials used, the application rates of binder and aggregates, condition of the existing pavement, and construction practices. These factors have a combined effect on the PE of aggregates, which has been used as a design parameter for chip seals to define a range of PE values corresponding to acceptable performance in terms of raveling and bleeding given climate and traffic conditions (Boz et al., 2019; Kim et al., 2018).

Several studies have listed different possible laboratory and field performance tests that can be incorporated in the QA of chip seal construction. Adams et al. (2019) proposed a guideline for performance-related specifications (PRS) for construction QA of chip seal surface treatments. The proposed PRS framework establishes acceptance quality characteristics (AQCs) related to chip seal performance measures. The AQCs included emulsion–aggregate adhesive strength measured using the Vialit test, gradation, and emulsion and aggregate application rates measured from the Vialit test samples separated in an ignition oven. The performance measures were aggregate loss and bleeding.

The study proposed the concept of percent within limits (PWL) to determine whether a chip seal treatment passes the PRS threshold values. Moreover, the study indicated that PWL may be used to establish warranty and construction incentive programs, which are frequently used in conventional asphalt pavement construction.

Other test procedures for aggregate loss of chip seal treatments have been proposed in previous studies using third-scale Model Mobile Load Simulator (MMLS3) testing (Kim & Adams, 2011; Lee et al., 2006; Lee & Kim, 2010). The studies found that if a chip seal surface exhibits 10% aggregate loss in the laboratory, it is likely to exhibit significant aggregate loss (based on visual inspection) in the field. The Alaska Department of Transportation also defines "acceptable" field aggregate loss as 10% or less for any traffic situation (McHattie, 2001). In another study, Kim and Im (2014) found that chip seal specimens tested using Vialit test specimens exhibit more aggregate loss compared to specimens tested using MMLS3 under the same conditions. The ratio of aggregate loss from Vialit to MMLS3 tests was between 1.38 and 2.00. Moreover, unmodified emulsions in chip seals exhibited more aggregate loss during the Vialit test compared to polymer-modified emulsions. Based on the laboratory test results and previous findings from Kim and Im (2014), Adams et al. (2019) proposed 20% aggregate loss as a threshold for low-volume traffic roads and 15% aggregate loss for high-volume traffic. The medium-volume traffic limit was selected as the average of the low- and high-volume traffic limits (i.e., 17.5% aggregate loss).

Pourhassan et al. (2023) performed a 13-month field observation of chip seals, where laboratory and field data were compared and correlated. Both a conventional (mineral aggregate) and eco-friendly rubberized chip seal with 25%, 50%, and 100% crumb rubber as aggregate were tested in the laboratory and in the field. The effects of different aggregate types, binder application rates, and crumb rubber contents were studied. Most of the macrotexture loss occurred in the first 50,000 passenger car equivalent loads. Using up to 50% replacement of mineral aggregate with crumb rubber did not significantly affect the raveling resistance but using more than 50% rubber impaired the raveling resistance. Moreover, the study indicated that the Pennsylvania and Vialit tests may not be suitable for assessing aggregate retention under traffic loads. According to their results, a higher binder application rate provides a higher embedment depth of the particles, resulting in a larger surface area of the aggregate in contact with the binder. This increased contact area between the aggregate surface and the binder leads to an improved bond. More small-size particles will fill more gaps between the larger particles, leading to the rise of the binder and higher aggregate embedment depth, which leads to higher bleeding susceptibility under traffic loads.

Impact of PE on Chip Seal Performance

The target PE of newly constructed chip seals varies between agencies with a typical range between 50% and 80%. Michigan Department of Transportation (MDOT) has a criterion of 70% PE. According to MDOT, traffic volume plays a significant role in determining the desired chip embedment. If there is a higher traffic volume, then less residue is needed, as traffic will ensure that the 70% embedment criteria is met. This lower residue amount may also prevent flushing or bleeding in the finished product.

Haider et al. (2021) used data acquired by Boz et al. (2018) to develop linear regression models between PE and raveling or aggregate loss and bleeding of chip seals. These linear regression models were used to formulate a performance-related specification for chip seal construction using PE as the acceptance quality characteristic. The maximum allowable aggregate loss limit of 40%, per MDOT specifications, was used to determine the minimum limit of PE values in the chip seals. The minimum PE limits to minimize aggregate loss were 58% and 56% for chip seals with natural and slag aggregates, respectively. The maximum allowable chip seal bleeding limit for both aggregate sources was determined based on bleeding failure in accelerated laboratory tests using the Hamburg wheel-tracking device. The maximum PE limits to mitigate bleeding were 71.5% and 69.3% for chip seals with natural and slag aggregates, respectively.

Kumbargeri et al. (2021) studied the effect of asphalt binder and aggregate application rates on the PE and aggregate orientation of chip seal aggregates via digital image analysis. They also investigated the impact of PE on aggregate loss. A series of hot-applied chip seal specimens with varying aggregate and binder application rates were prepared. Then, the PE and aggregate orientation of chip seal specimens were determined by digital image analysis using a MATLAB-based computer software package named CIPS, which was validated previously by Kutay et al. (2016). The study found that low amounts of binder application rates or excessive amounts of aggregate application rates can cause the aggregates to disorient from their flattest sides. This was especially true when excessive aggregate application rates led to multiple layers of aggregates, which leads to the lever and wedge effect. The research concluded that the optimum amount of aggregate is that which leads to the highest amount of aggregate lying on their flattest sides for the given aggregate and binder application rates. Moreover, for a given percent embedment value, the emulsion-based chip seals outperformed the hot-applied chip seals in terms of aggregate loss as well as bleeding performance.

Several researchers have also investigated different techniques such as multilinear regression and soft computing, digital image analysis, finite element method, adaptive neuro-fuzzy system, and artificial neural network to develop models for predicting the change of chip seal PE (Boz et al., 2019; Kumbargeri et al., 2018, 2019; Seitllari & Kutay, 2018). Boz et al. (2019) used a Hamburg wheel-tracking device to evaluate aggregate loss and bleeding of chip seal samples using two emulsion types (CRS-2M and CSEA) and two aggregate sources (slag and natural aggregates). Digital image-analysis techniques were utilized to quantify and analyze the laboratory test results with respect to PE and chip seal macrotexture. Based on their test results, the minimum and maximum PE thresholds for chip seals are established as 58% and 70%, respectively.

Seitllari and Kutay (2018) studied soft computing and multilinear regression techniques to develop models to predict the progression of chip seal PE. The model uses inputs such as cumulative equivalent traffic volume, Vialit test results, dust content of aggregates, and initial embedment depth. Multilinear regression, adaptive neuro-fuzzy system, and artificial neural network techniques were used to estimate the PE. The results indicate that while most of the proposed models were able to predict the PE reasonably, the artificial neural network model performed the best. Boz and Kutay (2018) also evaluated the effect of aggregate PE on chip seal behavior using a 2D finite element approach. The study involved preparation of chip seal samples and capturing side-view images of these samples. The images were analyzed and used to create finite element models. Finite element

analysis was then used to estimate the aggregate displacement and stress distribution due to traffic loads. The analysis showed that maximum displacement of the aggregates decreased with an increase in PE but followed an asymptotic trend for PE values greater than 50%. Tensile stresses at the aggregate–binder interface decreased significantly with an increase in PE.

Percent Embedment Measurement and Surface Characteristics

In constructed chip seals, a cross section for a core through a chip seal is typically more sophisticated than the one illustrated in Figure 1 (Jeong et al., 2020). The cross section shown in Figure 3 was acquired from this study, and it shows a range of aggregate sizes in the top layer. Moreover, the top aggregate penetration into the original pavement surface or the underlying chip seal application varied significantly, as illustrated by the green line. Generally, PE measurement and estimation procedures can be grouped under three categories: 1) direct measurements, including visual assessment of individual aggregates pulled from the surface and image analysis of cores and cross sections; 2) indirect estimation based on aggregate and emulsion application rates and general correlations with texture parameters, and 3) back-calculation based on surface measurements and knowledge of aggregate characteristics.
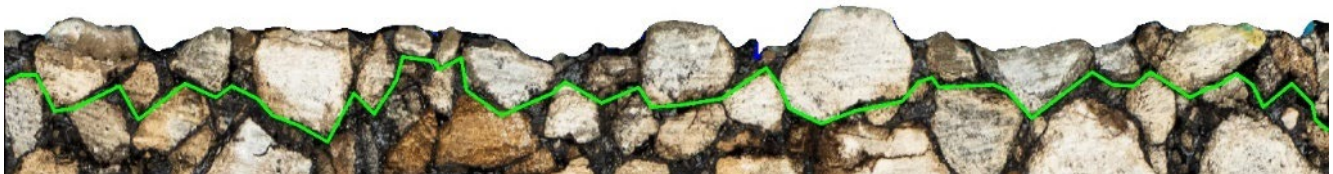
Figure 3. Photo. Chip seal cross section acquired from the field testing.

A research team at Michigan State University developed image-based analysis algorithms to measure PE from chip seal cross sections (Kutay et al., 2016; Ozdemir et al., 2018). The algorithms were implemented into a standalone software named CIPS developed in MATLAB. The main input is the digital image of the vertical cross section of the chip seal sample, and the main output of the analysis is the percent embedment and percent binder coverage. Although image-analysis techniques are accurate for individual cores, especially with careful QA, several definitions have been proposed to estimate percent embedment using image-analysis algorithms from cross sections, including the peak and valley method and the average PE value based on individual aggregate measurements (Kutay et al., 2016).

Previous studies have developed simplified procedures to estimate PE using average aggregate size, aggregates and emulsion or binder application rates, or voids between surface aggregates, which can be captured in mean texture depth measurements (Epps et al., 1980; Epps & Gallaway, 1972; Kearby, 1953). Other studies have indicated a potential link or correlation between the surface macrotexture and PE of chip seals (Kutay & Ozdemir, 2016). However, traditional texture measurements, including the mean profile depth (MPD) and mean texture depth (MTD), may not provide all parameters needed for calculating the PE for a wide range of chip seal materials and construction practices. Furthermore, texture measurements alone do not capture the effect of aggregate penetration into the substrate as well as the aggregate size distribution or orientation (Boz et al., 2019).

The sand patch method (ASTM E965) is one of the most used volumetric methods for macrotexture characterization (Chamberlin & Amsler, 1982). The sand patch test is performed by applying a known volume of sand and then using a measuring cylinder to pour it onto the road surface to form a cone. The sand is spread with a spreading disc to form a circular patch. The diameter is measured at four different angles by rotating 45 degrees between each measurement. Using the mean diameter and the sand volume, the MTD is defined as the ratio of the volume to the spread area. Although widely used, the sand patch method is operator dependent, time consuming, and requires traffic control (McGhee & Flintsch, 2003). To mitigate some of the shortcomings in the sand patch method, several non-contact surface profile tracing systems have been developed to acquire pavement surface texture. A wide range of texture parameters have been proposed using non-contact techniques include MPD, wavelets analysis, and power spectral density (Flintsch et al., 2021).

Based on the simplified definition of PE presented in Figure 1, agencies and researchers have proposed the possibility of using surface texture as a direct QA measurement. Gransberg and James (2005) indicated that measuring surface characteristics such as skid resistance and texture depth are repeatable and objective quantitative performance measurements of chip seals. The Indiana Department of Transportation used to rely on visual inspection for chip seal QA procedures. However, the time and labor required to perform visual inspection along with concerns of reliability and validity of the procedure motivated the agency to investigate the use of texture measurements in QA procedures for chip seal applications (Zhao et al., 2018). MPD was selected as the macrotexture metric to measure chip seal quality. Extensive testing was conducted on both test tracks and other chip seal projects to validate the use of the MPD metric as a cost-effective solution for chip seal construction QA. The study recommended performing a one-time QA inspection using MPD after the first snow of the season to ensure both safety and quality. Moreover, the study concluded that visual inspection is still necessary to identify problems earlier when corrective actions can still be taken and to avoid consequences due to immediate and dramatic loss of surface friction. The study recommended that visual inspection should be conducted before applying fog seal.

International transportation agencies in Australia, New Zealand, South Africa, and the United Kingdom measure surface texture using a sand circle test to characterize the existing pavement surface before chip seal application. These agencies also find it necessary to carry out surface hardness tests by using specialty testing equipment such as a penetrometer or ball penetration device to determine the nominal size of the aggregate to be used in their design methodologies. These sound engineering principles reduce the uncertainty and variability associated with chip seal design and construction as well as minimize field adjustments of binder and aggregate application rates (Gransberg & James, 2005).

In summary, several relevant methods have been found in the literature. Table 1 presents a summary of the tests and procedures to estimate PE for chip seals. The measured values varied between these methods and have been poorly correlated to ground truth readings in many procedures. Other methods including lab testing or image-based analysis are involved and require extensive testing procedures. Moreover, these controlled methods can be challenging to implement in the field during construction.

Table 1. Overview of QA Procedures Used During Chip Sealing Operation

PE Tests and Estimation Procedures	Relationship to Performance	Test Requirements	Accuracy, Precision, and Reproducibility	Notes	References
Image-based PE measurements	Good correlation with performance tests	Requires coring and advanced image analysis	Highly accurate and reproducible	The coring requirements can be challenging for field evaluation applications	Kutay et al. (2016); Ozdemir et al. (2018)
ALD machine measurement	Experience and practice documents relationship but limited quantitative evidence	Machine and data acquisition system	Highly accurate and reproducible for lab specimens but not in the field	Time consuming and not the most cost-effective solution	Dumas (2001)
Emulsion and aggregate application rates	Good correlations for highly controlled construction projects	Controlled laboratory and field tests Field and lab sampling before and during construction	Reasonably accurate for highly controlled construction Low reproducibility since it requires calibration for individual projects	Does not yield direct PE measurements but it relates to PE through iterative measurements Requires highly calibrated construction process	Jeong et al. (2020); Kim et al. (2018)
Pulling individual aggregates	Insufficient studies	Simple measuring tools in the field	Low representation of the construction site	Does not provide sufficient estimation for the entire site	Gransberg & James (2005)
Empirical correlations between texture parameters and PE	Good indication of performance but limited studies estimating relation to PE	Laser texture scanner or sand patch test	The texture measurements are accurate but the estimated PE values are not	Correlations are sparse and highly scattered	Adams & Kim (2014)

STATE SURVEY

To complement the literature review findings, 30 departments of transportation were contacted to provide additional insights on the current state of practice. The survey included three questions:

1. Are there specifications or requirements for an acceptable PE range?

2. What are the current guidelines or recommended procedures to quantify the PE?

3. Are there guidelines or recommended procedures to estimate the PE from surface texture measurements?

Twenty-four states responded to the questionnaire, as presented in Table 2. There are no established practices to measure PE in the field or as part of a QA program. Moreover, many agencies do not have established QA procedures or programs for chip seal construction.

Table 2. State Survey Results

	State	Response to Question 1	Response to Question 2	Response to Question 3
1	Alabama	No specifications	No specifications	No specifications
2	Arkansas	No specifications	No specifications	No specifications
3	Colorado	30-40% prior to rolling	Visual evaluation of pulled aggregates	No specifications
4	Connecticut	50% embedment for asphalt rubber and 50% to 60% for emulsion chip seal, following compaction	No specific guidelines	Although not related to PE, the texture meter is used when visible concerns arise for any project with unusual texture
5	Delaware	50% embedment from the spreader and 70% after final roll.	Visual evaluation of pulled aggregates	No specifications
6	Georgia	No specifications	No specifications	No specifications
7	Indiana	50% to 70%	Visual inspection	Research study recommends using macro-texture depth directly for QA without the need to estimate PE
8	Iowa	No specifications	No specifications	No specifications
9	Kansa	No specifications; however, designed to achieve 60% to 70%	No specifications	No specifications

	State	Response to Question 1	Response to Question 2	Response to Question 3
10	Michigan	No specification; however have a warranty program in place	No specifications	No specifications
11	Minnesota	No specifications	No specifications	No specifications
12	Montana	No specifications; however, have a warranty program	No specifications	No specifications
13	Nebraska	No specifications. Use a test strip to confirm uniform distribution of emulsion applied at the target rate.	No specifications	No specifications
14	New Hampshire	No specifications	No specifications	No specifications
15	New Mexico	No specifications	No specifications	No specifications
16	New Jersey	No direct specifications, it is implicitly controlled through design and construction.	No specifications	No specifications
17	North Carolina	50% to 70% determined from a test strip	Visual assessment	Not required, however there is interest in moving toward more objective procedures
18	North Dakota	No specifications	No specifications	No specifications
19	Ohio	66% chip embedment for acceptance	Visual evaluation of pulled aggregates	No specifications
20	Oklahoma	No specifications	No specifications	No specifications
21	Pennsylvania	If less than 50 percent, the Representative may require the application of a fog seal	No specifications	No specifications
22	South Dakota	Targets 70%	No direct procedure, mostly rely on design and construction procedures	No specifications
23	Tennessee	No specifications	No specifications	No specifications
24	Texas	No specifications	No specifications	No specifications

CHAPTER 3: DATA COLLECTION

The data collection program for this study was designed to capture surface texture measurements of chip seals and extract cores for measuring the ground truth values for PE from different chip seals constructed in the state of Illinois. The goal of this study is to develop a procedure to estimate PE for chip seals using texture measurements to serve as a QA measurement. The following sections outline the site selection, data collection procedures in the field, and data collection for acquired cores in a controlled environment.

SITE SELECTION

The field-testing program was performed over two years in 2021 and 2022. In coordination with Illinois Department of Transportation (IDOT), the field testing in 2021 was performed on 10 in-service chip seal sections in Illinois, as presented in Table 3 and Figure 4. As seen from Figure 4 and Table 2, the test sites covered a wide range of treatment ages and locations to capture different traffic volumes, materials used in these locations, and construction practices such as binder and chip application rate. According to the *IDOT Seal Coats (Oil & Chipping)* 2017 construction manual, there are 80 possible combinations of chip seals based on aggregate types, gradation, shape, and application method. However, the combinations shown in Table 3 represent the most common material types used in Illinois. Note that all underlying surfaces were hot-mix asphalt (HMA), and the chip seals were constructed with one lift of chips (A-1) as opposed to double chip seal applications (A-2). Figure 5 presents two sites tested in 2021 showing vastly different conditions that were evaluated in subsequent tests and procedures.

Table 3. Field Testing Sites Evaluated in 2021

Site Number	County	Treatment Type	Underlying Pavement	Age	Type of Aggregate	Gradation	Bituminous Material
1	Piatt	A-1	HMA	<1	Steel slag	NA	NA
2	Knox	A-1	HMA	<1	Limestone	CA 16	HFRS-2P
3	Sangamon	A-1	HMA	3	Stone Cr CLAQ	CM 16	HFP
4	Sangamon	A-1	HMA	3	Stone Cr CLAQ	CM 16	HFP
5	Logan	A-1	HMA	3	Stone Cr CLAQ	CM 16	HFE GR 150
6	Logan	A-1	HMA	3	Stone Cr CLAQ	CM 16	HFE GR 150
7	Sangamon	A-1	HMA	2	NA	NA	NA
8	Hamilton	A-1 (2)	HMA	1	Stone Cr CLAQ	CA 16	PG46-28
9	Hamilton	A-1 (2)	HMA	3	Stone Cr CLAQ	CA 16	PG46-28
10	Hamilton	A-1 (2)	HMA	3	Stone Cr CLAQ	CA 16	PG46-28
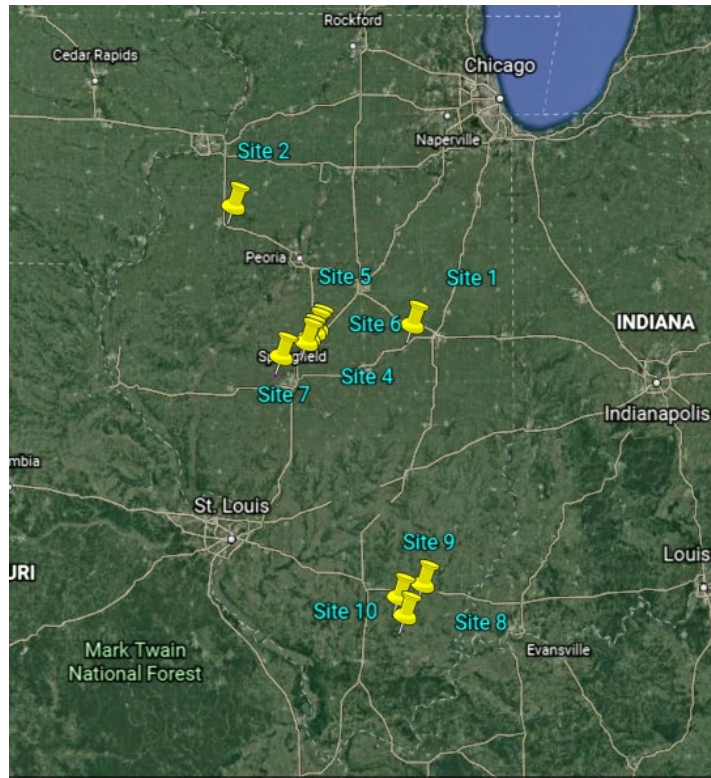
Figure 4. Photo. Test sites visited in 2021.

Figure 5. Photo. Chip seal surfaces from the test sites showing a newly constructed site in good condition (left) and one site with excessive bleeding (right).

The 2022 field testing included a construction project on a road segment along Illinois Route 116 near Roseville. The construction project was part of another research study on chip seals and included a wide range of aggregate gradations and bituminous materials, as presented in Table 4. Note that some of the sections were constructed with a steel roller, which is an uncommon practice in Illinois. In addition to the construction project sections, five in-service sections were also tested in Knox

County, Decatur, and Urbana to further validate the test procedures. Including the sites tested in 2021 and 2022, the study involved 24 test sections.

Table 4. Field Testing Sites Evaluated in 2022

Section	Direction	Bituminous Material	Aggregate	Steel Roller
1	East	CRS-2P	FA 4 PS&G	No
2	East	CRS-2P	FA 4 PS&G	Yes
3-E	East	CRS-2P	CA 16	Yes
3-W	West	HFRS-2P	CA 16	Yes
4-E	East	CRS-2P	CA 16	No
4-W	West	HFRS-2P	CA 16	No
5-E	East	CRS-2P	CM 16	No
5-W	West	HFRS-2P	CM 16	No
6	West	HFRS-2P	CM 16	No

FIELD TESTING DEVICES AND PROCEDURES

At each site, the tests were performed within 152 m (500 ft) test sections marked using reflective tape at the beginning and end of the section. As illustrated in Figure 6, the field tests included high-speed texture profiles acquired on the left and right wheel paths. Three repetitions of the high-speed texture profiles were acquired at 56 kmh (35 mph) for each site. Following the high-speed texture profiles, handheld stationary laser texture scans were acquired at 15, 76, and 137 m (50, 250, and 450 ft), measured from the beginning of the test sections. In 2021, additional stationary laser texture scans were acquired on the right wheel path at the same stations. Moreover, the 2021 testing program included sand patch tests performed at the same locations following the handheld texture scans in the right wheel path. Finally, cores were extracted for the handheld scanning locations in the right wheel path to be used for additional texture scans, cross section image acquisition, and overhead image analysis.

High-Speed Texture Profiler

The high-speed texture profiles were acquired using a Model 8300 High Speed Inertial Profiler manufactured by Ames Engineering. The profiler was front mounted on a truck with a standard 5 cm (2 in.) receiver hitch (Figure 7). The system was equipped with Ames AccuTexture 100 scanners on both wheel paths. The texture scanner acquires data at 100 kHz using an elliptical laser spot, which can be limited when used on tined surfaces. The system can collect measurements at speeds between 16 and 64 kmh (10 and 70 mph). For this study, all high-speed data were collected at 56 kmh (35 mph). Texture profiles were acquired from both wheel paths. Testing included three repetitions, and the start and end of each section was marked with reflective tape to trigger the high-speed profiler.
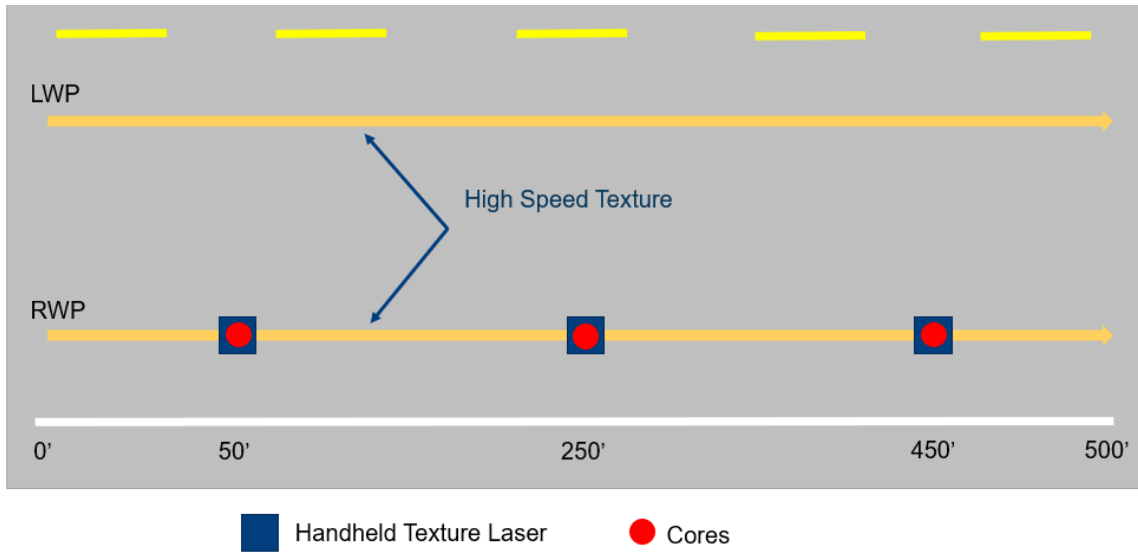
Figure 6. Sketch. Schematic of the field-testing layout.

Figure 7. Photo. High-speed texture profiler used in field testing.

Stationary Texture Measurements

Stationary texture scans were acquired using a 9400HD Laser Texture Scanner (LTS) from Ames Engineering shown in Figure 8. Using LTS 9400HD, the scanned area for all test points was 71.61 × 101.60 mm (2.82 × 4.00 in.). The scanner acquires single-point measurements along 100 line scans with a spacing between the points within each line of $6.35 × 10^{-3}$ mm ($0.25 × 10^{-3}$ in.) and a total length of 101.60 mm (4.00 in.). The spacing between the line scans was set to 0.72 mm ($2.84 × 10^{-2}$ in.). This allows researchers to capture macrotexture and a part of the microtexture of the scanned area in the longitudinal direction. The scanner uses a red laser with a dot size of $25 × 10^{-3}$ mm ($9.84 × 10^{-3}$ in.) at the center of range, with a 22 degree triangulation angle at the center of range. The

acquired points are then processed in a triangulation analysis algorithm to produce a 3D point cloud of the surface texture, as presented in Figure 8. After scan completion, the scanner calculates and displays the MPD and estimated texture depth (ETD) on the sunlight-readable LCD display. The research team took note of those readings and downloaded the completed scan data to validate the readings using the accompanying software. The scanner and software estimates MPD and ETD in accordance with ASTM E1845.

It should be mentioned that some of the 2022 construction sites were not evaluated using the handheld laser texture scanner due to safety concerns for performing tests during construction. The extracted cores from these sites were scanned in the workshop during the controlled data acquisition phase. Following the scans, the sand patch test was performed at the three texture scanning patches on the right wheel path for the sites tested in 2021 (Figure 9). The tests were performed in accordance with ASTM E965-15. The test was performed using glass beads meeting AASHTO M 247-13 Type II requirements.
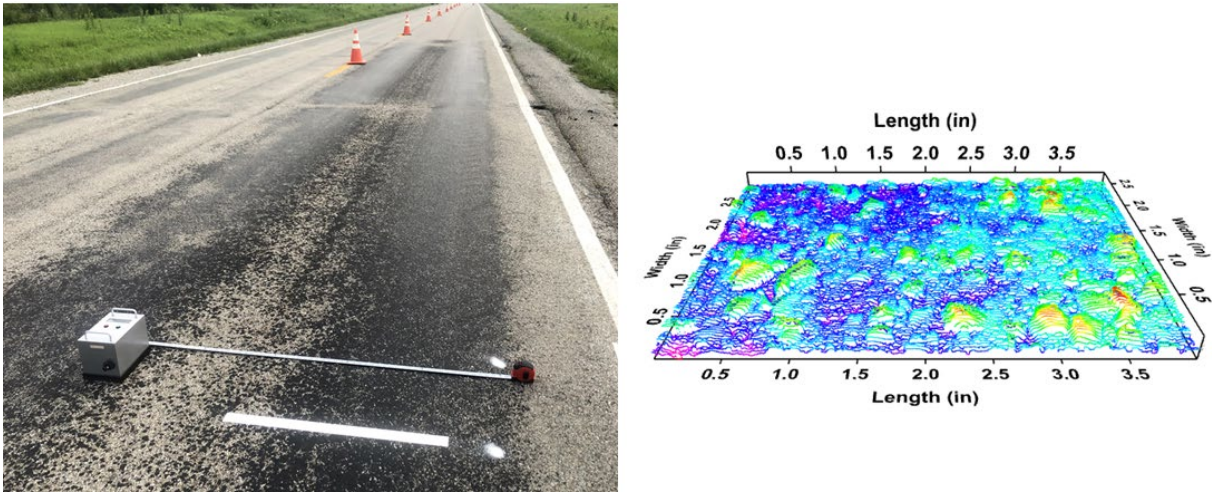
Figure 8. Photo and Plot. Texture measurement using the handheld laser device.

Figure 9. Photo. Sand patch test performed in the field.

Core Samples

After completing the texture measurements, a 152.40 mm (6 in.) rotary diamond coring bit was used to extract three cores from the same scanning patches in the right wheel path for all test sites (Figure 10). The coring machine was advanced slowly to minimize the distortion and misplacement of the aggregates in the chip seal layer. In 2021, the coring location was cooled by placing an ice bag on the surface to minimize the sample distortion due to emulsion/binder flow at summer temperatures. In addition to ice bags at the surface, a water supply tank was filled with water and ice to keep the water at a low temperature during the coring process. The cores were then rinsed and placed in airtight bags, marked and labeled directly after coring, and then placed in a cooled box to prevent/minimize core damage, especially the surface chip seal layer. The cores were shipped back to temperature-controlled storage at ARA's workshop to be fabricated for the controlled data acquisition phase.

Figure 10. Photo. Coring operation (left); picture of a typical core (right).

CONTROLLED DATA ACQUISITION

The first step in the controlled data acquisition was to trim the acquired cores into squares, as shown in Figure 11. This shape reveals four sides that can be used in measuring ground truth PE values from the image analysis of side photos and allows for rescanning the cores' surfaces and acquisition of overhead photos.

Figure 11. Photo. Core prepared for controlled data acquisition.

Side-View Photos

As shown in Figure 12, the trimmed cores were placed on a flat surface with blue playdough applied on top of the trimmed core to improve contrast and provide sharper color change between the top of the core and the background for image analysis. A measuring tape below the cross section and a ruler to the left side of the cross section were included in the photo to scale the pixel size and transform the photo dimensions to actual length dimensions. The cores shown in Figure 12 were acquired from a construction project in 2022. As seen in Figure 12, the emulsion/binder is smeared on the top layer of the cross section. This smear covered some of the aggregates and limited the number of detected aggregates using the image-analysis algorithms developed in this study. Moreover, some of the aggregates were crushed due to the steel roller application in some of the cores.

All side-view photos were compiled and labeled in a laboratory and then reviewed to ensure the cores were centered and had uniform lighting conditions. Moreover, the photos for cross sections constructed using dark color slag or had excessive emulsion/binder smear were excluded from the analysis if the algorithms could not yield consistent aggregate and binder detection. The distance from the camera to the cores and the camera settings were consistent for all cores, with slight variations in the final resolution and dimensions, as presented in Table 5.
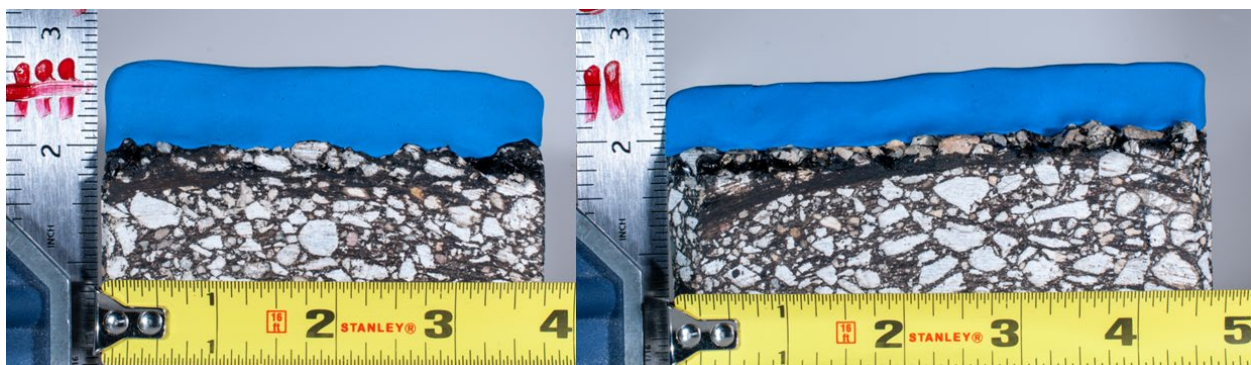
Figure 12. Photo. Side-view photos of trimmed cores showing the cross section of the chip seal layer and the underlying pavement layer.

Table 5. Side Image Characteristics for All Cores Included in the Study

	Number of Core	Number of Images	Original Image Resolution in Pixels (width × height)	Cropped Image Resolution in Pixels (width × height)	Pixel per mm
Phase 1 (2021 testing)	31	124	7360 × 4912	2100~2200 × 500~600	21.01 (0.0475 mm/px)
Phase 2 (2022 testing)	54	216	3700~3850 × 2400~2550	2200~2500 × 450~6050	26.31 (0.038 mm/px)

Overhead Images and Cores Texture Scanning

In addition to the side images, the research team rescanned all acquired cores with the handheld LTS 9400HD in the workshop. The rescanned cores were used to verify the field texture measurements, provide texture data for the construction sites that were challenging to scan in the field, and acquire high-density scans to assess the minimum scan densities for chip seal evaluation. Moreover, overhead images were acquired for the cores to be used later in the overhead image-texture analysis, which provides a potential alternative for ground truth PE estimations.

To provide consistent overhead scans and images, the team designed and built the overhead scanning-imaging acquisition frame shown in Figure 13, which can be used for cores in the workshop and direct surface measurements in the field. A sketch of the frame design with dimensions can be found in Appendix A. The frame includes an outside box to prevent excessive light from the sun and provide consistent lighting conditions using a camera flash or other lighting sources. At the bottom, the setup includes a scanning rack consisting of four beams holding a black scanning plate with an opening corresponding to the scanning window of the LTS 89400 HD scanner. The scanning window is surrounded by graduated straight edges on two sides, as shown in the left photo of Figure 14. The scanning plate at the bottom is part of the LTS 9400HD scanner accessories. The height of the scanning rack can be adjusted to allow for a core below the rack or to be as close as possible to the road surface if used in the field. The laser texture scanner was placed on the scanning plate during data collection to have a consistent scanning window at the same location.

Following the texture scans, the camera was attached to a second adjustable rack above the scanning rack and brought closer to the core, as shown in Figure 14. The advantage of keeping the scanning plate on the scanning rack is to expose the chip seal surface only through the scanning window in the overhead photos. This helps match the 3D scans and the overhead photos to create color-coded 3D images. As seen in Figure 15, the scanning window is slightly larger than the actual scanned area; however, it still provides a much smaller window in the photos to be matched with the 3D scans.

Table 6 provides a summary of the overhead images' characteristics acquired in the overhead scanning-imaging acquisition frame. All acquired images had consistent resolution and dimensions due to the fixed frame position.

Table 6. Overhead Image Characteristics for All Cores Included in the Study

	Number of Core	Number of Images	Original Image Resolution in Pixels (width × height)	Cropped Image Resolution in Pixels (width × height)	Pixel per mm
Phase 1 (2021 testing)	31	31	4288 × 2848	2820 × 2020	27.70 (0.0361 mm/px)
Phase 2 (2022 testing)	54	54	4288 × 2848	2820 × 2020	27.70 (0.0361 mm/px)

Figure 13. Photo. Overhead scanning-imaging acquisition frame designed and built in this study.
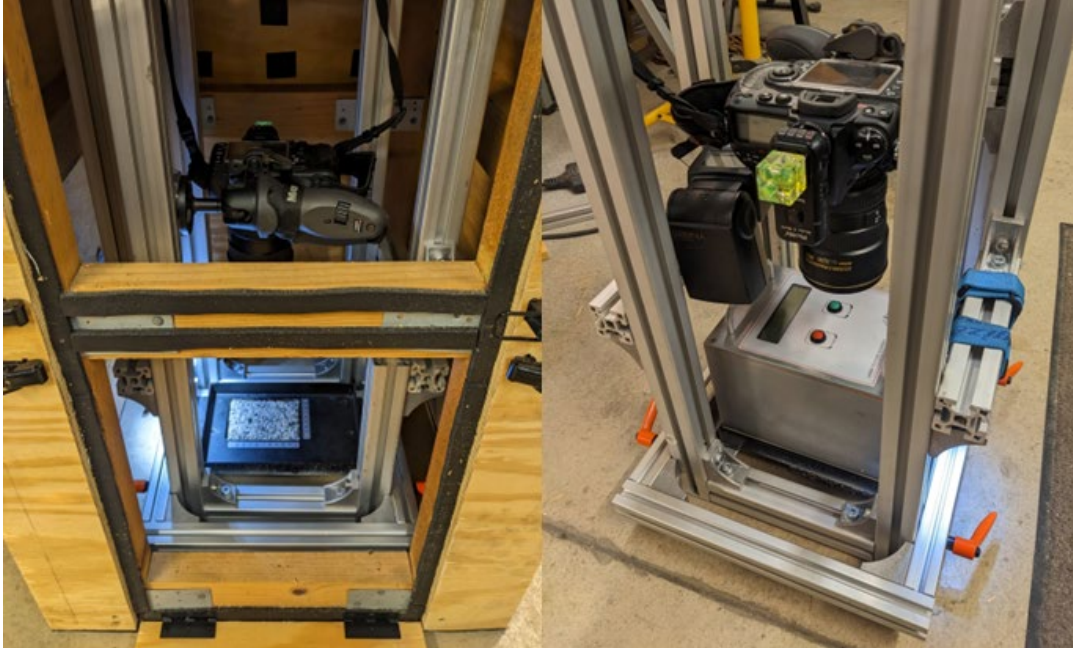
Figure 14. Photo. Overhead scanning-imaging acquisition frame details with the camera and scanner in position for data collection.
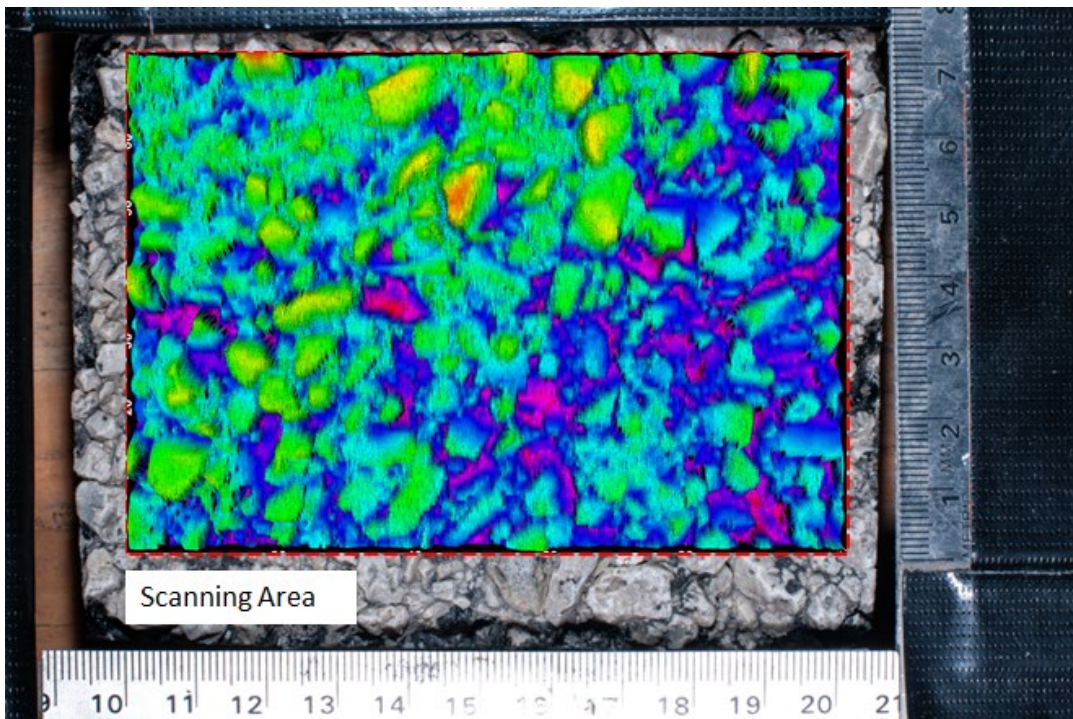
Figure 15. Photo and plot. An overlapped texture scan and overhead photo acquired in the scanning-imaging acquisition frame.

CHAPTER 4: DATA PROCESSING AND ANALYSIS PROCEDURES

The data processing and analysis procedures performed in this study were divided into three major themes depending on their role in the study:

- Surface texture analysis from the stationary laser texture scans and the high-speed profiles.

- Side-view image analysis for calculating ground truth PE values and texture analysis.

- Overhead image-texture analysis for estimating PE.

LASER-BASED SURFACE TEXTURE ANALYSIS

Stationary Laser Texture Scans

The first step in analyzing the stationary laser texture scans was to export the initial analysis results from the software provided by Ames Engineering and the point coordinates to be further processed. The initial outcomes from the Ames Engineering software include the mean profile depth (MPD) and estimated texture depth (ETD) in accordance with ASTM E1845, average roughness (Ra), root mean square roughness (Rq), skewness (Rsk), and kurtosis (Rku). Although the collected scans include a 3D point cloud of the surface area, the analysis in the software is limited to algorithms processing the lines individually then averaging these line measurements across the area. Additional 3D analysis algorithms have been developed in this study as part of the overhead image-texture analysis procedure. Using the exported point clouds, the research team performed wavelet and power spectral density analyses in Python to compare the spectral content from the stationary scans and high-speed texture profiles.

Power Spectral Density

Power spectral density (PSD) is the most frequently used method for analyzing pavement texture in the frequency domain using Fourier transform (FT) analysis. It describes how the energy of a pavement texture profile is distributed over different frequency ranges. The analysis starts by applying FT to individual lines in the scan to decompose it into a series of sinusoidal functions with discrete frequencies, represented using the wave number ω, and the corresponding amplitudes. Following that, PSD can be calculated by normalizing the square of the complex absolute value of the FT for a given wave number band.

In addition to the fundamental concepts described herein, additional processing is required to estimate PSD for surface texture data, as outlined in Table 7. Figure 16 shows a sample PSD plot on a log-log scale. Note that PSD follows a linear trend on a log scale. This is a common trend for a wide range of rough surfaces. When the power spectral densities are calculated with a constant bandwidth method, their representation in a log-log diagram give an appearance or visual impression at high frequencies, which over-emphasizes the fluctuations of PSD generated by the real power distribution and by the statistical noise. For this reason, PSD shall also be represented in a smoothed form (i.e., by the mean PSD in one-twelfth-octave bands).

Table 7. List of Steps for PSD (modified from ISO/TS 13473-4, 2008)

Step	Result
Anti-aliasing filtering	Analog signal
Digital sampling	Digital signal sampled at intervals Δx ($= v/f_s$) (v = measurement speed, f_s = sample rate)
Interpolation of dropouts	Digital signal with interpolated values at dropouts
Offset suppression	Digital signal with zero average
Slope suppression	Digital signal with zero slope
Windowing	Finite sampled signal with length $l = \Delta x\, N$ (l = evaluation length, N = number of samples)
Discrete Fourier transform (fast Fourier transform)	Complex spectrum with constant bandwidth $\Delta f_{sp} = 1/l$ at frequencies $0 \dots (N-1)\,\Delta f_{sp}$ (Δf_{sp} = spatial frequency (in m^{-1})
Transformation to power spectral density	Power density spectrum with constant bandwidth $\Delta f_{sp} = 1/l$ at frequencies $0 \dots (N-1)\,\Delta f_{sp}$
Transformation to constant relative bandwidth spectrum	Profile level spectrum with constant-percentage bandwidth
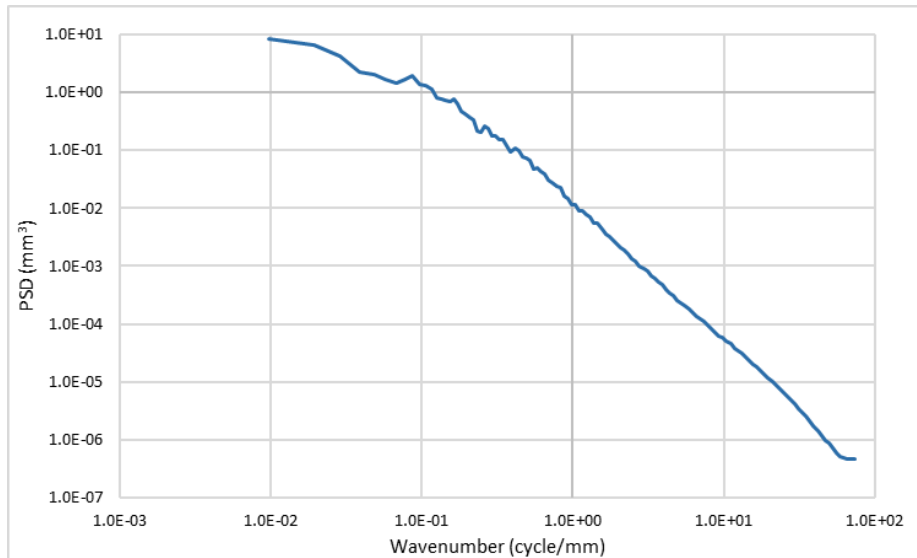
Figure 16. Graph. PSD for a line in a texture scan from a chip seal surface.

Wavelet Analysis

Wavelet analysis provides an alternative description of the spectral content for surface texture profiles. Wavelets, which can be thought of as wave pulses that translate and dilate in the spatial domain, are used as building blocks to overcome the time–frequency resolution issue arising from Fourier transform. Discrete wavelet transform bases are constructed iteratively and must satisfy a set of admissibility conditions. Wavelet families constitute a sequence of sub-profiles collectively for the full profile space. Wavelet families differ from each other, and each family has a different trade-off

between how compact and smooth the wavelet looks. The PyWavelets(pywt) package contains 14 mother wavelets. Based on previous studies, Daubechies wavelet families are the most common application in surface texture analysis, which is composed of 10 compactly supported orthonormal wavelet functions (db1, db2, db3, …, db10). Several studies have used db3 mother wavelets to analyze pavement surface texture, roughness, and degree of aggregate segregation. Symlet wavelets are the improved version of dbN. Accordingly, Daubechies(db3) and Symlets(sym5) are selected for analysis in this study (Alhasan et al. 2020; Yang et al. 2018; Zelelew et al. 2014).

High-Speed Texture Profile Analysis

High-speed texture profiles were first processed using the Ames Engineering software package to filter the profiles and estimate MPD for segments of the profile. The profiles were then exported to estimate PSD and compare the stationary texture measurements to high-speed texture profiles. The profiles were marked using markers from the reflective tape applied in the field to find 152 m (500 ft) long segments and mark the location corresponding to the stationary texture scans. The texture profiles were divided into ~15 m (49 ft) segments, and the segment containing the stationary scans was used in the comparison.

SIDE-VIEW IMAGE ANALYSIS

To calculate the percent embedment of chip seals using side-view images, a total of 340 images were collected from 85 cores with four sides for each core. Figure 17 illustrates the process that was followed to develop the side-view image analysis. All processing algorithms were implemented in Python. The details of each step are described in the following subsection. Appendix B provides pseudocodes for all algorithms developed for the side-view image analysis.
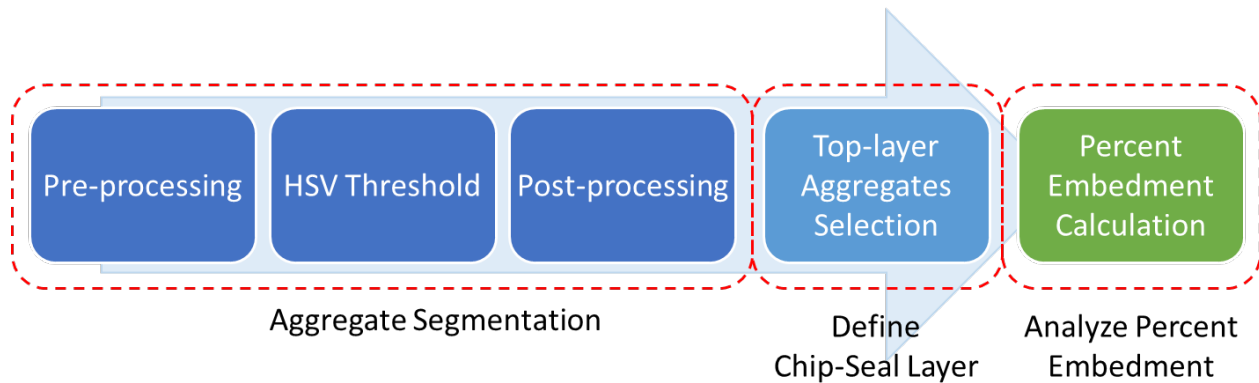
Figure 17. Graph. Algorithm framework for the side-view image analysis.

Pre-processing

In the preliminary stage of the side-view image-analysis procedure, a series of pre-processing steps were executed to enhance the quality of the acquired images. These steps aimed to mitigate potential artifacts and improve the accuracy of subsequent analyses. Slope suppression using linear regression for surface angle correction and Gaussian blur were applied in that order.

- *Slope Suppression:* A linear regression fit was employed to correct any angular variations present in the collected images. Because the surface of the specimen/core have diverse angles and orientations, such variations could potentially introduce errors for MPD calculation from side-view images and PE calculations. Applying linear regression effectively mitigated angular irregularities, as shown in Figure 18, ensuring a more consistent alignment of the surface in the images.

- *Gaussian Blur:* After the angle correction, a Gaussian blur correction filter was implemented to facilitate noise reduction and image smoothing. Noise, including pixel-level variations, could impact the precision of the subsequent analysis processes. The Gaussian blur filter was employed to suppress high-frequency noise while preserving essential features of the image.
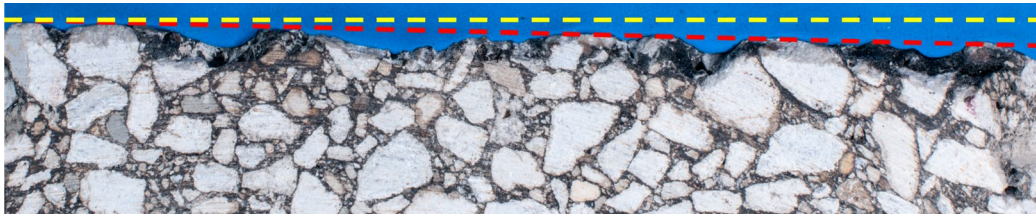
A. Original side-view image before slope suppression
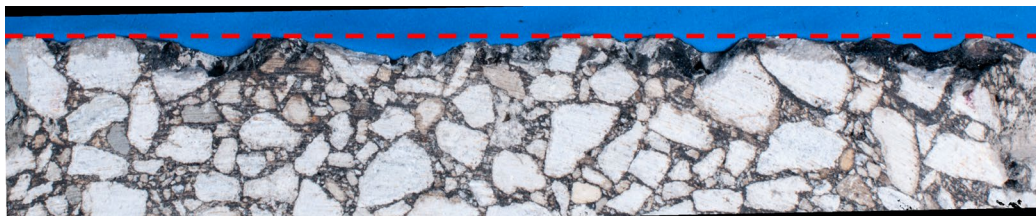
B. Side-view image after slope suppression

Figure 18. Photo. Side-view image slope suppression.

Hue, Saturation, Value Thresholding

The segmentation of aggregates from the background and the binder in the side-view images requires the application of thresholding to separate the image into regions based on their color. Thresholding poses several challenges, such as the high complexity of aggregate distribution, and the inherent limitations of traditional thresholding methods. The following is a brief description of HSV (hue, saturation, value) thresholding as an alternative to the traditional method to address the segmentation issue and improve the accuracy of aggregate segmentation.

- *Traditional Threshold Methods*: Traditional thresholding methods, such as Otsu's method and adaptive thresholding, are widely employed for image segmentation tasks. However, these methods encounter difficulties in distinguishing individual aggregates from the background within our data, as illustrated in Figure 19-A. Aggregates have a close grayscale intensity to the surrounding background (binder), and this similarity results in challenges in achieving precise segmentation results.

- *HSV Threshold*: HSV color representation separates color information into distinct components: hue, saturation, and value. This separation provides additional color characteristics of the aggregates that can distinguish it from the background. Better performance in aggregate segmentation was observed by employing the HSV threshold method compared to traditional methods, as illustrated in Figure 19-B. The thresholds were then fine-tuned manually for individual images to achieve optimal results for aggregate segmentation using the HSV threshold tool.
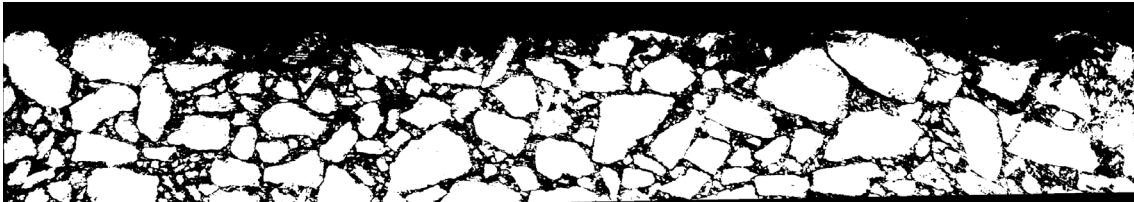
A. Side-view image after traditional Otsu's thresholding method
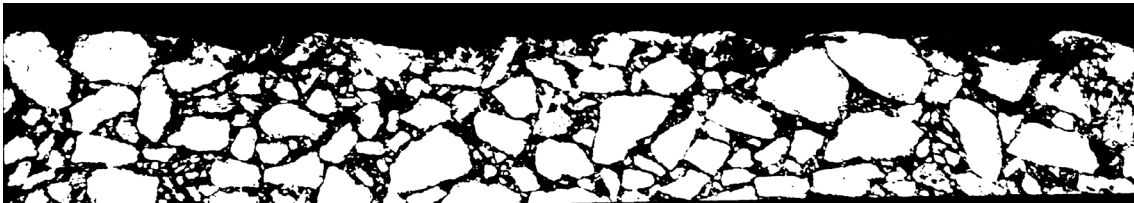
B. Side-view image after HSV thresholding method

Figure 19. Graph. Side-view image thresholding.

Post-processing

After segmenting the images, a series of post-processing techniques were applied to refine the segmentation results. The goals of post-processing were to eliminate noise, enhance image quality, and address issues arising from the interconnectedness of individual aggregates that are supposed to be separated resulting from the initial morphological operations. The two post-processing steps employed to achieve these goals are described below.

- *Morphological Image Processing (Dilation and Erosion)*: To mitigate the presence of noise and improve the quality of the segmented images, a combination of dilation and erosion operations was applied. Dilation was executed to fill small gaps and irregularities present within the aggregates. Subsequently, erosion was employed to counteract the dilation effect and restore the original size and shape of the aggregates while reducing the impact of noise.

- *Watershed Algorithm*: One of the challenges encountered during and after morphological processes was the formation of interconnected aggregates due to the proximity of aggregates or their compacted structure in 3D. This interconnectedness greatly affects the accuracy of the PE analysis results, because small individual aggregates are recognized as one large aggregate. To address this issue, the watershed algorithm was introduced. The watershed algorithm leverages the concept of treating intensity gradients in an image as topographical

features. By considering these gradients, the algorithm can accurately segment regions that might otherwise appear connected, as shown in Figure 20.
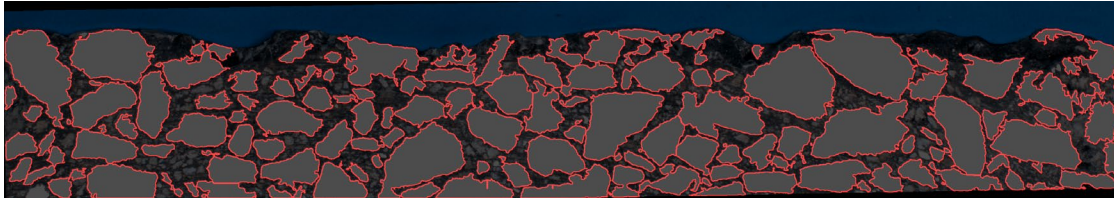
Figure 20. Graph. Side-view image after post-processing.

Top-layer Aggregate Selection

The following step in the analysis pipeline involved the selection of top-layer aggregates, which are assumed to correspond to the chip seal layer. This manual process was driven by specific criteria designed to define the chip seal layer of aggregates for further analysis.

- *Aggregate Numbering and Positioning*: Each individual aggregate was assigned a unique identification number based on its position within the image as shown in Figure 21-A. This numbering was based on the x and y coordinates of the center of each aggregate, effectively creating a representative label that could be used to identify the aggregates spatially.

- *Top-Layer Aggregate Selection*: Based on the observation, an initial range of aggregates that corresponded to the top layer were specified. This specific range of aggregates may represent the spatial information of the chip seal layer and its expected thickness. To accurately identify the chip seal layer from the initially selected aggregates, aggregates that lay beneath others were excluded from the final list of top-layer aggregates as shown in Figure 21-B. This was done by analyzing the spatial relationships of aggregates based on their assigned identification numbers. Each calculation method was built into a method in a Python environment, enabling efficient and automated analysis.
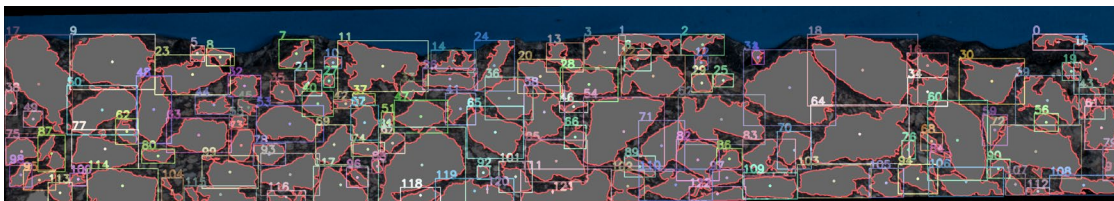
A. Side-view image after aggregate numbering and positioning
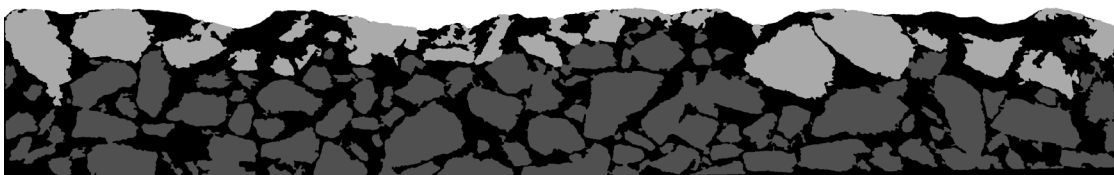
B. Side-view image with top chip seal layer identification

Figure 21. Graph. Side-view image after aggregate numbering and top layer selection.

Percent Embedment Calculation

There are four possible approaches to calculate PE using the identified top aggregate layer:

- Average elevation method

- Percent embedment of each aggregate method

- Peak method

- Aggregate circumference method

Average Elevation Method

In this method, the chip seal surface within the image is divided into binder and aggregate segments, as shown in Figure 22. Accordingly, the average elevation of the points in the binder segments is then divided by the average elevation of the points in the aggregate segments. Because the actual underlying surface is hard to identify from the images, the elevation is measured from a reference line at the deepest aggregate point for the surface layer aggregates. This method is robust, as determining the binder and aggregate segments at the top of the image is most accurate and consistent compared to labeling individual aggregates.

Figure 22. Photo. Side-view image with binder and aggregate separation at the surface.

Percent Embedment of Each Aggregate Method

In this method, individual PE values are estimated by dividing the average two binder heights surrounding the individual aggregates, measured from the bottom of the aggregate, by the height of the individual aggregate, as illustrated in Figure 23. The height of the aggregate in a constructed chip seal is typically equal to the least dimension. The overall percent embedment can be calculated as the average of the individual PE values for the individual aggregates. This method can be robust for newly constructed sections because it is insensitive to the reference line. However, the method can be sensitive if small-size aggregates are included in the calculations.
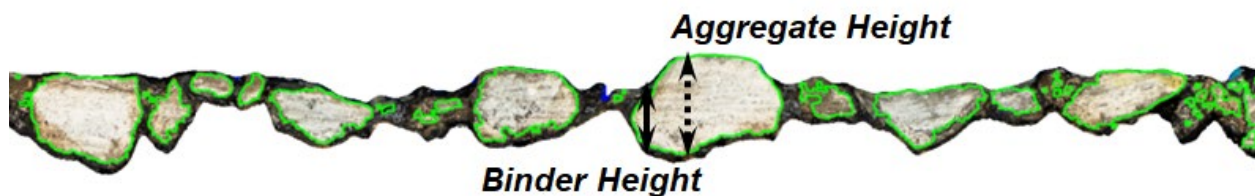
Figure 23. Photo. Side-view image for measuring individual aggregate PE.

Peak Method

In this method, the average peak elevation of individual aggregates is divided by the peak elevation of the binder surrounding the aggregates. The elevations are measured from the reference line at the deepest aggregate point for the surface layer aggregates.

Aggregate Circumference Method

In this method, PE is estimated for individual aggregates and then averaged for all aggregates in the top layer as shown in Figure 24. The PE values for individual aggregates are estimated using the equation shown in Figure 25. This method can be useful in estimating the area adhering to binder, which relates to raveling susceptibility, but it may have poor correlations with bleeding susceptibility.

Portion of Agg. Circumference NOT Covered with Binder, C_s (i.e., Exposed at surface)

Portion of Agg. Circumference Covered with Binder, C_b (i.e., NOT exposed at surface)
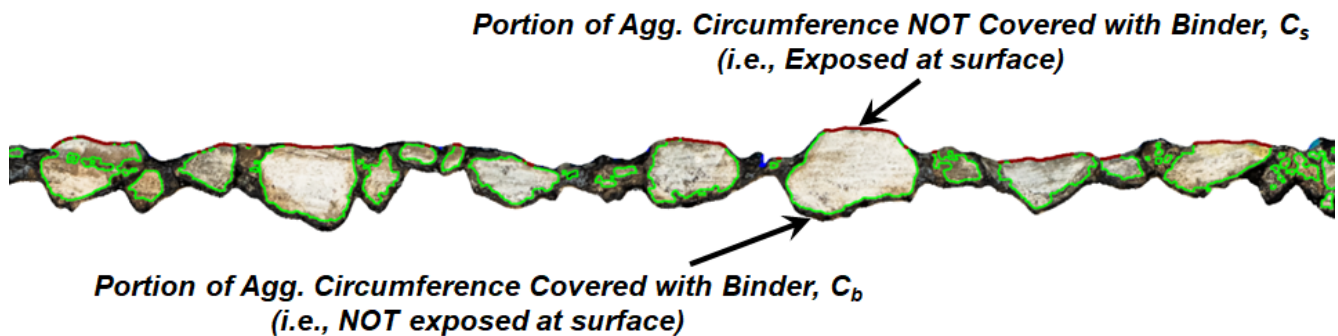
Figure 24. Photo. Side-view image for measuring PE using aggregate circumference method.

$$PE\left(\%\right) = \frac{c_b}{\left(c_s + c_b\right)} \times 100$$

Figure 25. Equation. Estimation of PE for individual aggregates using circumference method.

Texture Characterization from Side-View Images

In addition to the PE calculations estimated from the side-view images, texture analysis was performed to estimate MPD, in accordance with ASTM E1845, and the average least dimension of the individual aggregates in the top aggregate layer. These values were estimated by transforming the pixel size to actual dimensions by scaling the pixel size using the reference measuring scales included in the acquired images, as shown in Figure 12.

OVERHEAD IMAGE-TEXTURE ANALYSIS

To overcome the need for coring in the field to perform the side-view image analysis, an analysis method was developed to process the overhead images and texture data acquired using the frame discussed in Chapter 3. To analyze PE of chip seals using overhead images, a total of 97 images and corresponding texture data were collected using a prototype data acquisition setup. Figure 26 illustrates the process that was followed to develop the overhead image-texture analysis method. Appendix C provides pseudocodes for all algorithms developed for overhead image-texture analysis.
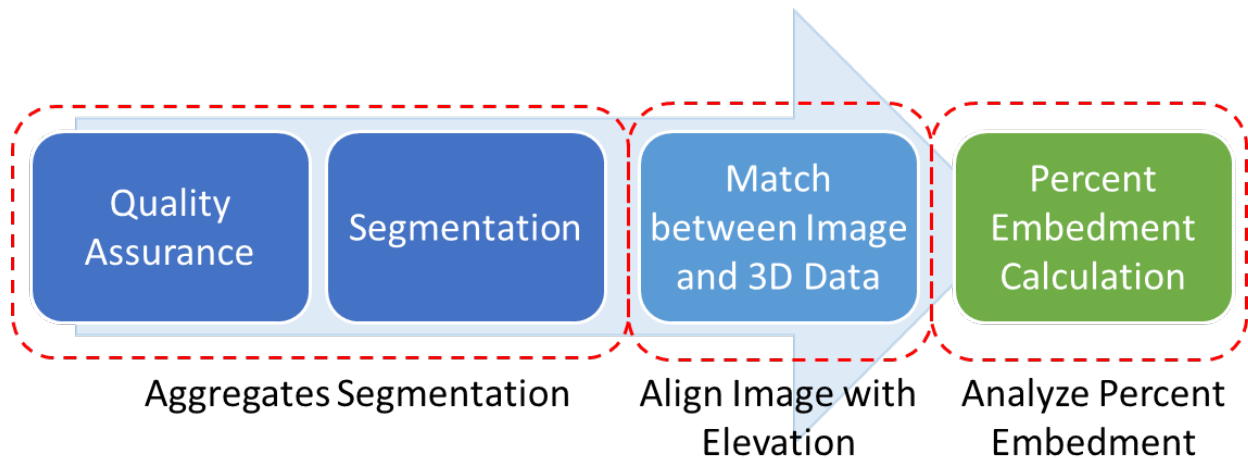
Figure 26. Flowchart. Proposed overhead image-texture analysis algorithm framework.

Quality Assurance and Data Preparation

As described in Chapter 3, the acquisition of images and texture data was performed using the prototype data acquisition setup shown in Figure 13 and Figure 14. The data acquisition setup ensured consistent data collection, allowing for easy matching between images and texture scans. To ensure the reliability and accuracy of the collected data and preparation for the subsequent processes, a series of quality assurance and data preparation steps were implemented.

- *Resolution and Camera Position Consistency*: A critical aspect of the QA process involved confirming the consistency of the resolution and camera position for all collected images. This step was crucial to ensure all data were collected under the same setting. To ascertain camera positions, individual images were reviewed and checked in reference to the graduated straight edges on the two sides of the scanning window. The pixel size was scaled using the graduated straight edges and confirmed to be consistent for all images.

- *Image Cropping for Correspondence*: Because the scan area of the LTS and the area captured by the camera are different, images were cropped by finding the corresponding areas with LTS, as shown in Figure 15. Considering the scanning area dimensions of 101.6 mm (4.00 in.) along the x-axis and 71 mm (2.80 in.) along the y-axis, a cropped image size of 2,820 pixels by 2,020 pixels was determined to match the scan. This calculated size ensured that the cropped images accurately represented the relevant pavement surface area while maintaining the required resolution for accurate analysis.

Segmentation

To segment the individual aggregates from the background in the overhead images similar to the one shown in Figure 27, the research team implemented the thresholding and segmentation algorithm used in the side-view image analysis. Moreover, a state-of-the-art deep learning–based segmentation model was implemented and compared to the thresholding approach.

- *HSV Threshold Approach:* Similar to the side-view image analysis, the HSV threshold method was initially employed to separate the pixels corresponding to aggregates from the binder pixels. However, this approach proved to be highly sensitive to color properties, and its effectiveness was limited, as illustrated in Figure 28. Some of the challenges included aggregates of varying colors, small- and large-size aggregate variation, presence of overlapping aggregates, and poor contrast of aggregate boundaries. The complexity of overhead images greatly affected aggregates' segmentation performance.

- *Segment Anything Model:* To address the limitations of the HSV threshold approach and enhance the aggregates' segmentation performance, a novel artificial intelligence (AI) model named the "Segment Anything Model" (SAM) was implemented. SAM was developed by the Meta AI research team and released as an open source code (Kirillov et al., 2023). This model was developed using an efficient model in a data collection loop, built with over 1 billion masks on 11 million licensed and privacy-respecting images. The model represents a significant leap in segmentation capability, boasting considerable power and versatility. Contrary to conventional AI models, SAM stands out due to its self-supervised technique. This technique grants SAM the ability to perform large-scale training without necessitating traditional training datasets. As a result, SAM exhibits robust performance without the need for extensive training. Figure 29 presents a segmented overhead image in Figure 27 using the SAM model. The model outperforms the traditional HSV threshold approach with lower noise. SAM was implemented and tailored for this project in Python.

Figure 27. Photo. Overhead image acquired for newly constructed chip seal.
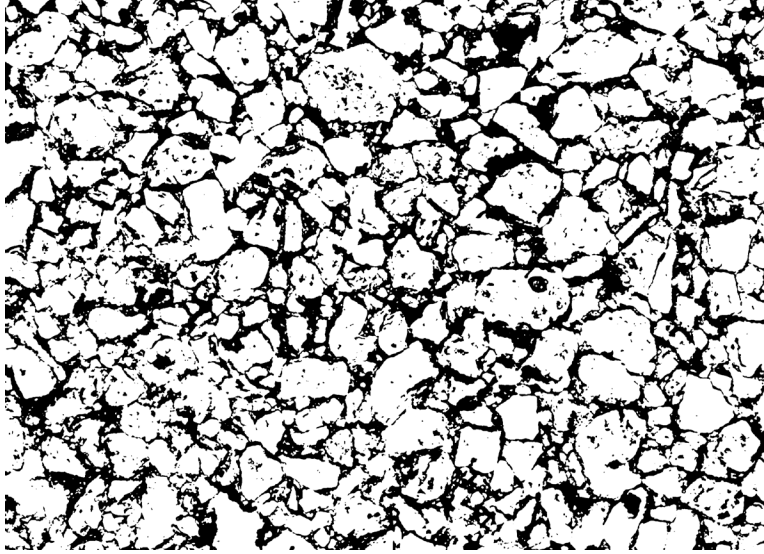
Figure 28. Graph. Segmented overhead image using HSV threshold approach.
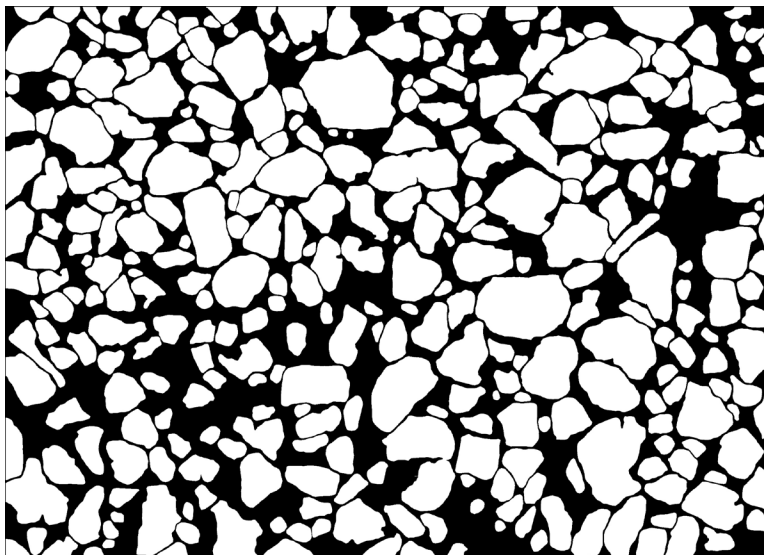
Figure 29. Graph. Segmented overhead image using the SAM model.

Overhead Image and 3D (LTS) Data Matching

As discussed previously, the cropped top-down image measures 2,820 pixels in length and 2,020 pixels in width, while the LTS data comprise 16,004 data points along the x-axis (length) and 101 data points along the y-axis (width). The discrepancy in dimensions poses a challenge when attempting to match the two datasets effectively. In particular, the length resolution of the image presents an issue, as each pixel on the y-axis corresponds to a range of 20 data points from the LTS data. This matching can potentially lead to a loss of valuable information in the y-axis direction.

To overcome this challenge, a 2D interpolation technique was employed to expand the LTS data. The original LTS data of 16,004 × 101 were transformed into a shape of 16,004 × 2020. The interpolation

technique reduced the amount of data in the LTS corresponding to a single pixel on the y-axis of the images. This adjustment ensured a more appropriate alignment between the image and the 3D LTS data.

Percent Embedment Calculation

After aligning the segmented overhead images with the corresponding 3D LTS data, the elevation values corresponding to the coordination of the image were extracted. To focus the analysis on larger size aggregates, only the top 20% of aggregates were included in the analysis. The top 20% of aggregates were then labeled as shown in Figure 31.

- *Exposed Height Calculation*: To estimate the percent embedment of individual aggregates, the exposed height was calculated for individual aggregates from the LTS data measured relative to the height of the surrounding binder. This exposed height represents the difference between the highest elevation points of an aggregate and the average elevation of its boundary (i.e., embedding binder).

- *Percent Embedment Calculation*: The PE for individual aggregates is calculated using the equation shown in Figure 30.

$$PE(\%) = \frac{ALD - |h_b - h_h|}{ALD} \times 100$$

Figure 30. Equation. Percent embedment calculation using overhead image-texture analysis.

Where, h_b is the average elevation of aggregate boundary, h_h is the highest elevation of aggregate, and *ALD* is the average least dimension. *ALD* is derived from the side-view image analysis and represents the average height of the chip seal aggregates. The overall PE was then estimated as the average of the PE values of individual aggregates.
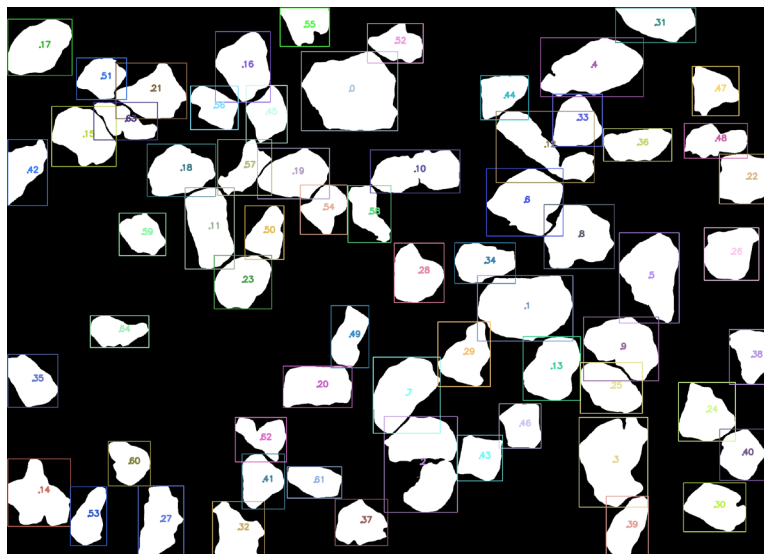
Figure 31. Graph. Labeled 20% aggregates.

CHAPTER 5: RESULTS AND DISCUSSION

This chapter documents the results and findings from all analyses and observations from the field testing and data collection discussed in Chapters 3 and 4.

TEXTURE CHARACTERISTICS

Stationary Texture Measurements

To characterize the chip seal surface texture, the following parameters were calculated for individual lines in the stationary texture scans:

- Mean profile depth (MPD)

- Arithmetic mean deviation (Ra)

- Root mean square (RMS)

- Skewness (Rsk)

- Wavelet energy and power spectral density (PSD)

All parameters were then averaged for the lines in the scan to provide an average characteristic value for each scan. Figure 32 through Figure 34 present the scatterplots and regression models correlating MPD to Ra, RMS, and Rsk estimated using the stationary laser texture scanner for all sites. The correlations are relatively weak, indicating that each texture parameter represents different surface characteristics. Moreover, Figure 32 through Figure 34 showed different trends between Phase I and Phase II data, which correspond to in-service and newly constructed chip seals.
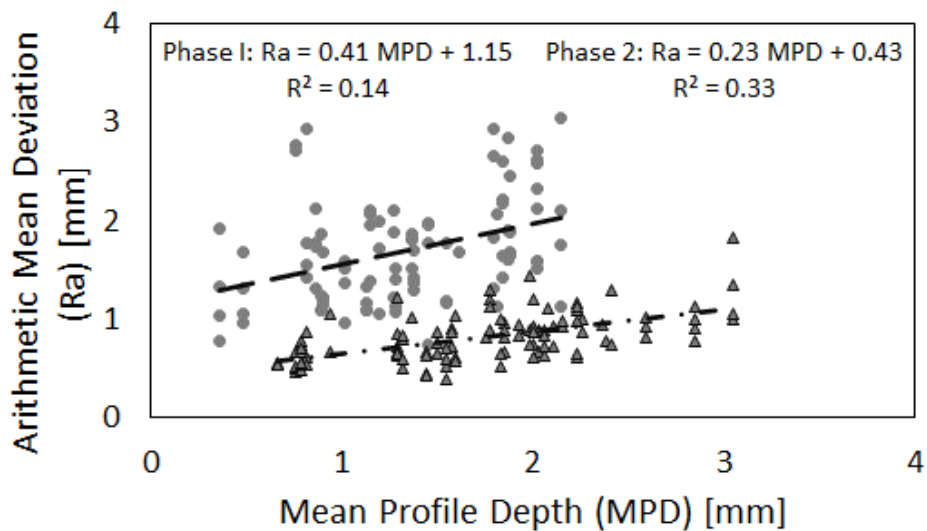
Figure 32. Plot. A scatterplot and regression models between MPD and Ra.
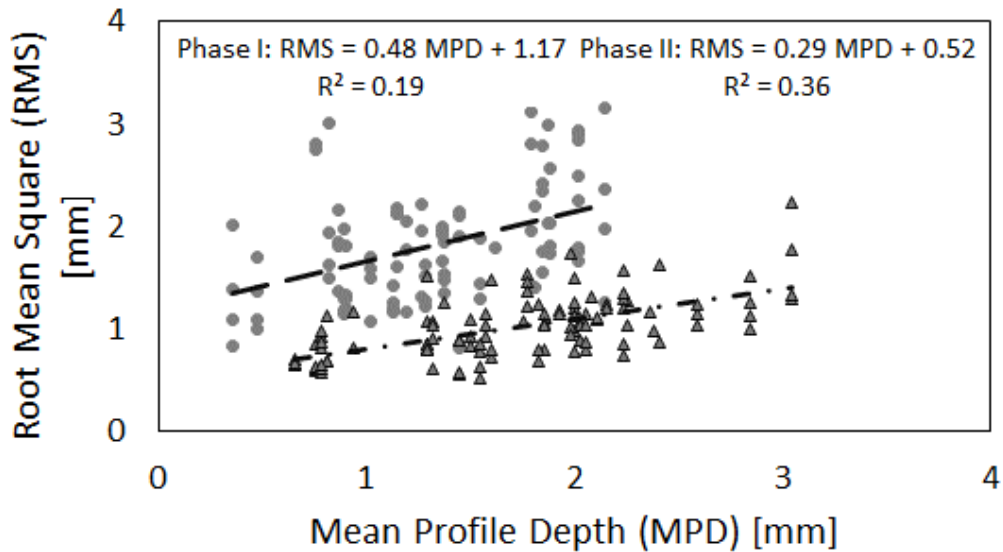
Figure 33. Plot. A scatterplot and regression models between MPD and RMS.
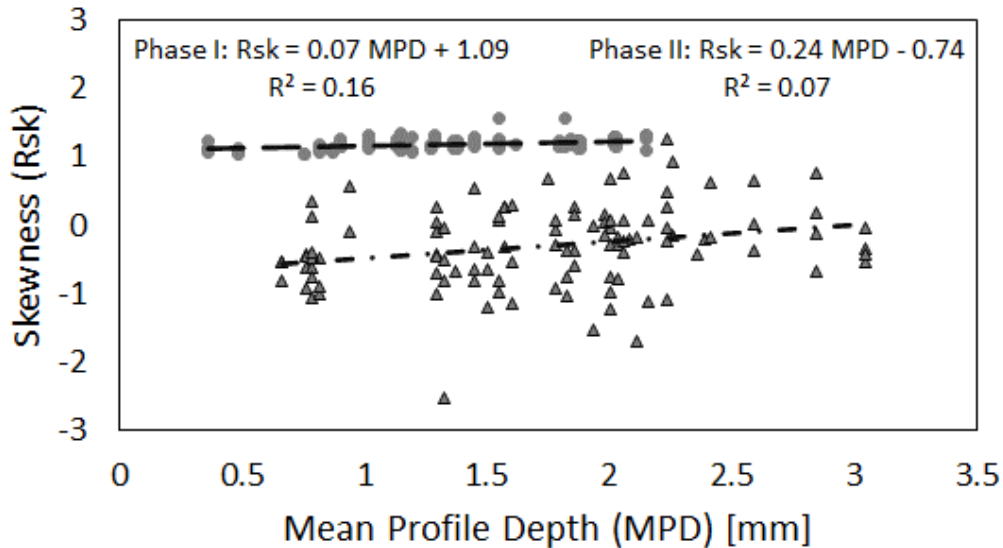
Figure 34. Plot. A scatterplot and regression models between MPD and Rsk.

To evaluate the minimum scan density requirements, 10 full high-density scans were processed to sample the data points down. The high-density scans included 2,917 lines with 16,000 points acquired in each line. The scanning time for the full high-density scans is approximately 3.5 hours, and the file size can be significantly large to be processed effectively. In comparison, the scanning time to acquire 100 lines with the maximum number of points in each line is approximately 12 minutes. Figure 35 shows that the average MPD estimated using 100 lines with the maximum number of points is equivalent to the average MPD estimated using the full high-density scans. Moreover, the other texture parameters did not change significantly.

Figure 36 presents the change in MPD estimated using 100 lines with different reduction rates for the points in the individual lines. The data reduction was performed by sampling out the points from individual scan lines and estimating the MPD values from the down-sampled line scans. As seen in Figure 36, the change in MPD starts slow and accelerates after 50% reduction. Moreover, the analysis shows that the change in MPD after 20% data reduction ranged from 1% to 3% compared to the full scan line data. The change in MPD after 40% data reduction ranged from 3% to 8% compared to the full scan line data.

$$MPD_{100} = 0.9413\ MPD_{High} + 0.0557$$

$$R^2 = 0.988$$
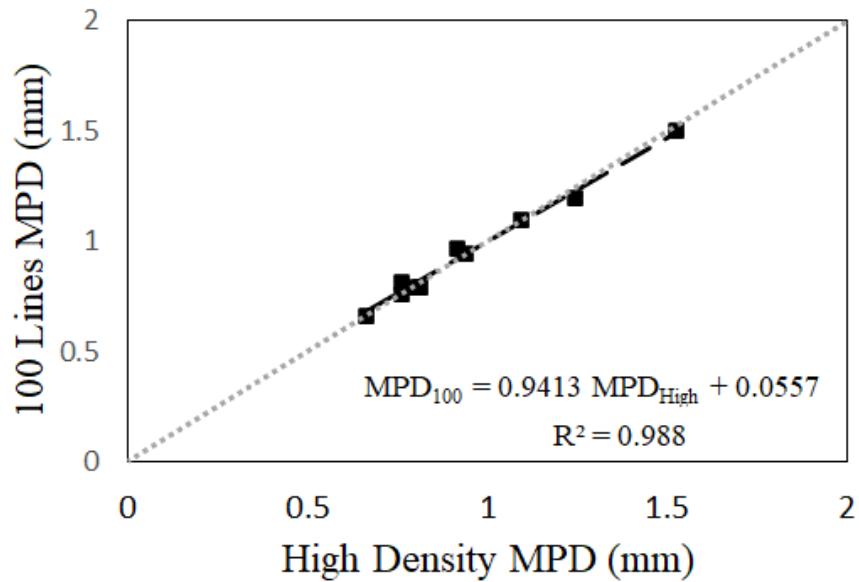
Figure 35. Plot. MPD estimated using scans with 100 lines versus the full high-density scan.
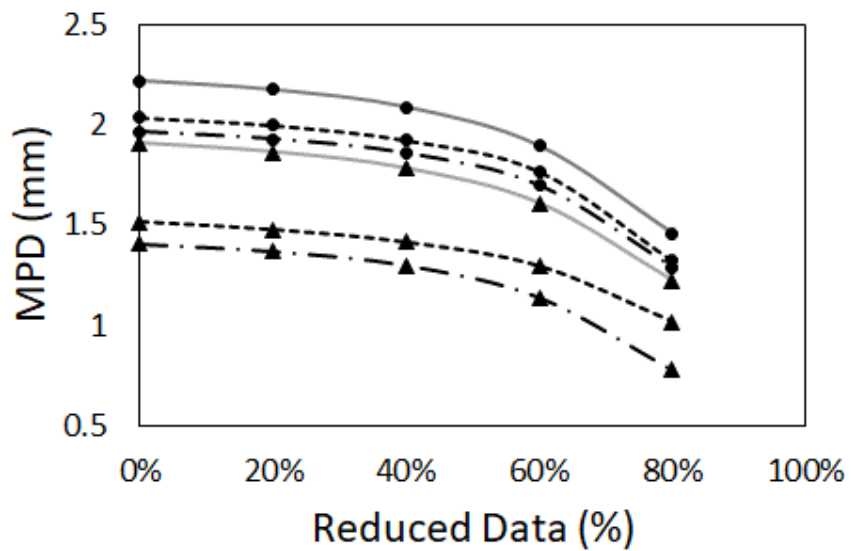
Figure 36. Plot. Change in MPD for different data reduction rates from the individual scan lines.

High-Speed Versus Stationary Texture Measurements

As mentioned in Chapters 3 and 4, a high-speed texture profiler was also used to characterize the chip seal surface texture. The high-speed texture profiles were segmented into shorter segments. The segments containing the stationary scans were further analyzed to estimate the texture parameters discussed in the previous section. Figure 37 presents the texture characteristic parameters estimated from one site using the stationary laser texture scanner and the corresponding segments from the high-speed texture profiler. From the analysis, MPD estimated from the high-speed profiler had a 6% to 50% difference from the MPD values estimated using the stationary scanner. The other texture parameters from the high-speed texture profiler were up to 20 times greater than the ones calculated using the texture scanner.
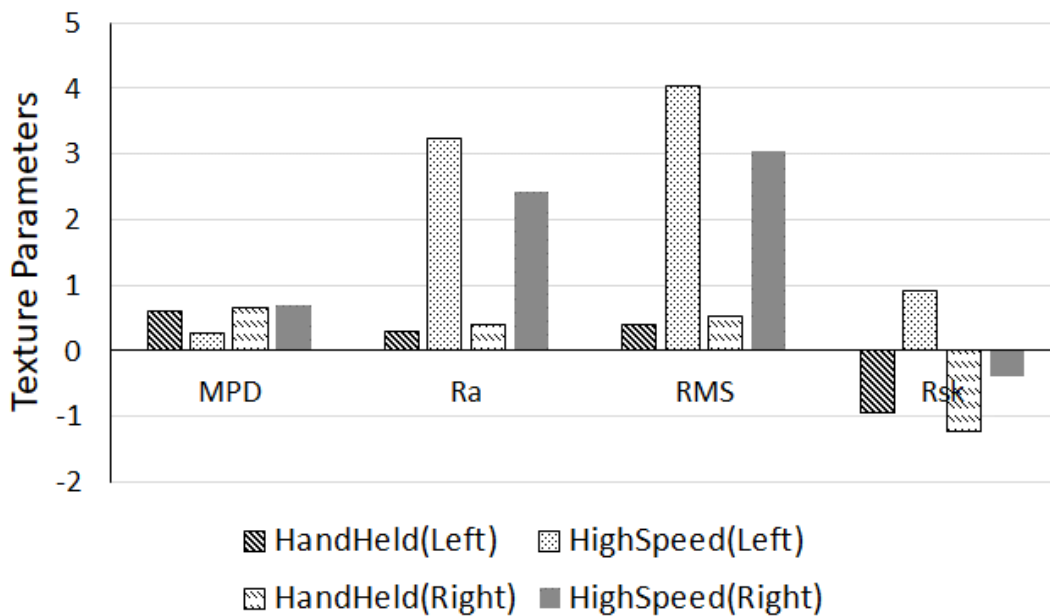
Figure 37. Graph. Texture indices from stationary and high-speed texture scans.

In addition to the surface texture parameters, the PSD from the stationary scanner and high-speed profiler are shown in Figure 38. Due to the different sampling intervals and profile lengths, the wave number range is different for the two systems. However, they overlap between 0.0096 to 0.8934 1/mm wave number ranges. In some profiles, the PSD produced by the high-speed texture profiler produced a PSD that is very close to the ones produced by the stationary scanner, such as the right wheel path high-speed profile in Figure 38. Other high-speed texture profiles exhibited significantly different PSD from the stationary texture scanner PSD, such as the left wheel path high-speed profile in Figure 38. Note that the ripples at high wave numbers in the PSD drive can be due to windowing or segmentation of the full profile.
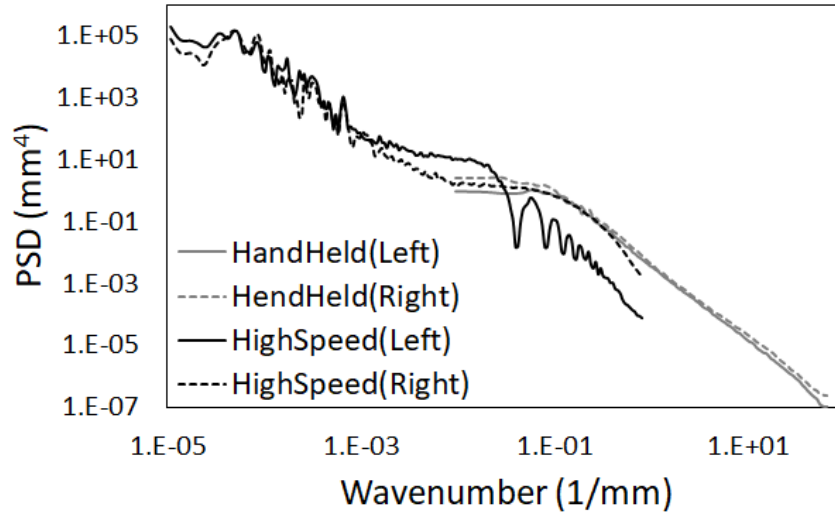
Figure 38. Graph. PSD for high-speed and stationary laser texture measurements.

Texture Characterization from Side-View Images

In addition to laser texture measurements, surface texture was characterized by calculating the MPD from the side-view images of the retrieved cores. This allowed the research team to relate the MPD to the PE values for each side image separately as opposed to using the average MPD for the 100 lines acquired from the core surface. Figure 39 presents the MPD estimated using the individual side images versus the average MPD estimated from the core surface. The high variability, and accordingly low R^2 values, are expected since the plots and regression line are comparing the MPD from one profile to an average MPD from 100 lines. Figure 40 presents the reduction in variability and improved correlation when using the average MPD calculated for the four side images versus for each core.
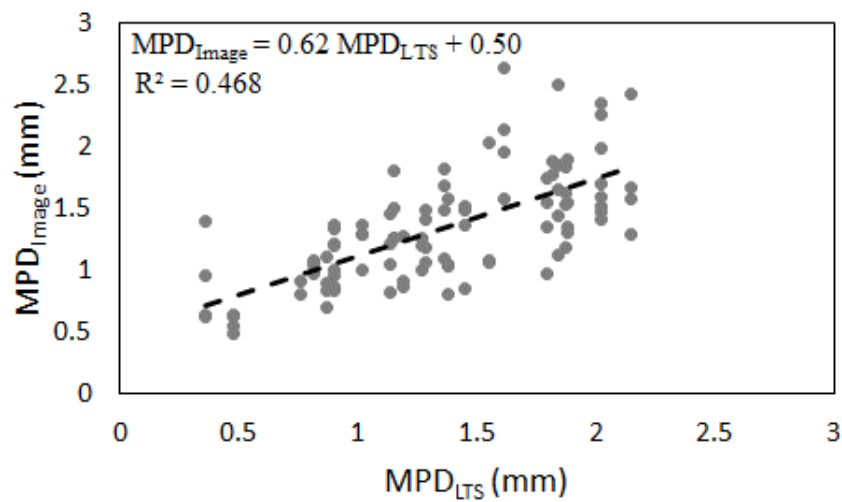
A. MPD calculated using side-view images and laser texture scans acquired for Phase I sites tested in 2021.
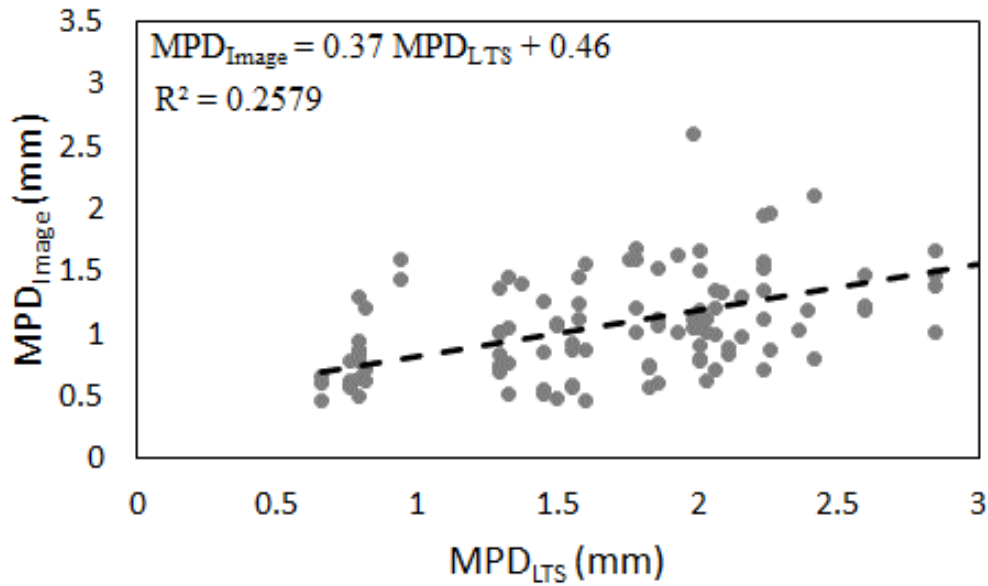
B. MPD calculated using side-view images and laser texture scans
acquired for Phase II sites tested in 2022.

Figure 39. Plot. MPD calculated using side-view images versus the average MPD calculated using laser texture scans.
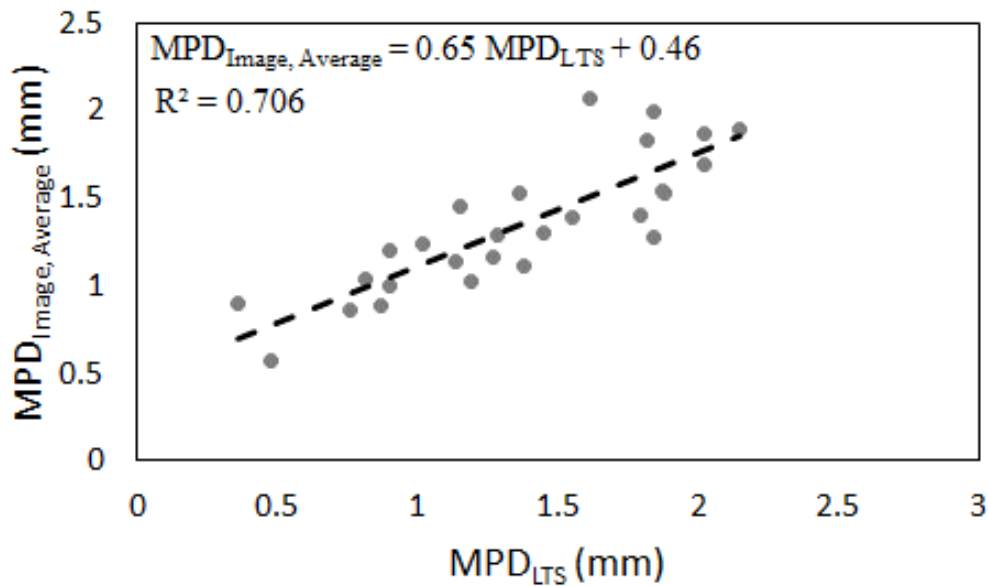
A. MPD calculated using the average of four side-view images and the
laser texture scans acquired for Phase I sites tested in 2021.
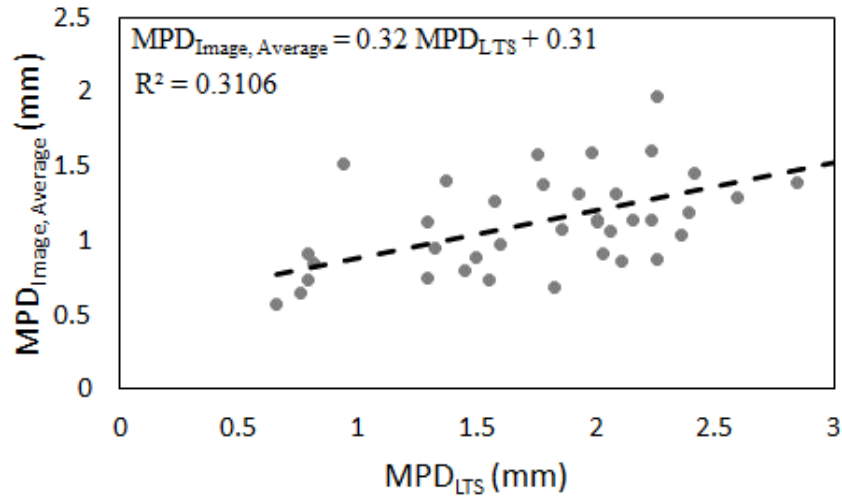
B. MPD calculated using the average of four side-view images and the laser texture scans acquired for Phase II sites tested in 2022.

Figure 40. Plot. MPD calculated using the average of four side-view images versus the average MPD calculated using laser texture scans.

SIDE-VIEW IMAGE ANALYSIS AND PERCENT EMBEDMENT CALCULATIONS

Using the side-view images, PE was calculated using the four methods discussed in Chapter 4. Figure 41 and Figure 42 present scatterplots and regression lines correlating PE values estimated using different methods. Except for Figure 42-C, the correlations are relatively weak, indicating the methods provide different information and may relate to different characteristics. It is notable that although the overall trends are consistent between Phase I and Phase II data, the regression equations are significantly different for the same regression variables. That variability can be attributed to the different construction practices and the fact that cores acquired in Phase II had emulsion smeared over some aggregates, which has a major impact on PE estimations.
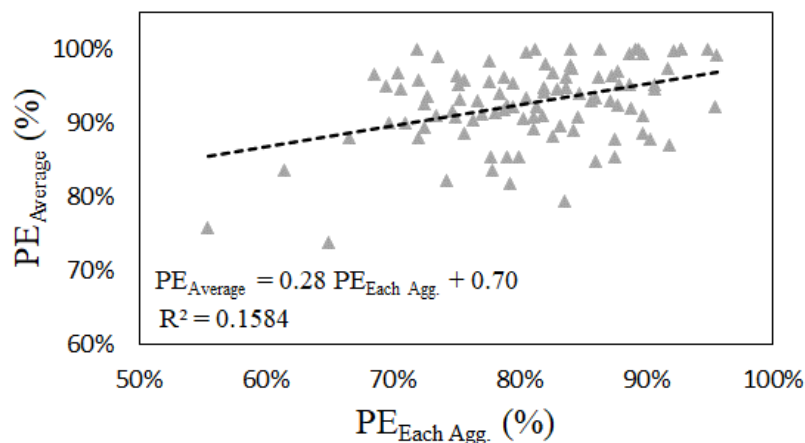
A. PE estimated using the average method versus each aggregate method
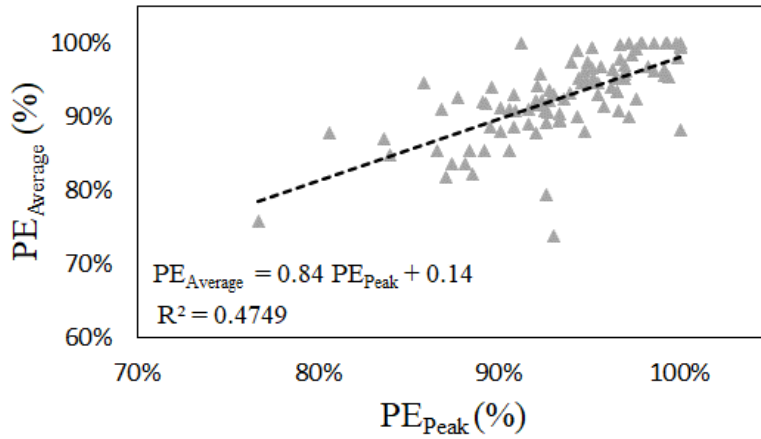
B. PE estimated using the average method versus peak method
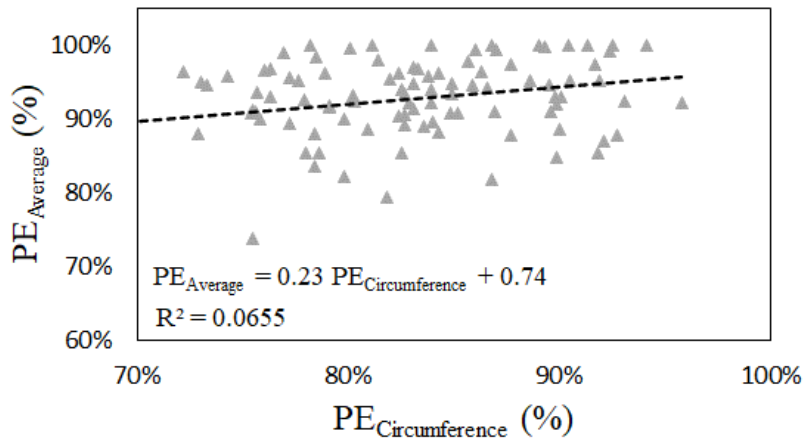
C. PE estimated using the average method versus circumference method

Figure 41. Plot. Scatterplots with regression lines of PE values estimated for Phase I sites.

A. PE estimated using the average method versus each aggregate method

$$PE_{Average} = 0.31 \, PE_{Peak} + 0.62$$

$$R^2 = 0.2114$$

B. PE estimated using the average method versus peak method

$$PE_{Average} = 0.62 \, PE_{Circumference} + 0.35$$

$$R^2 = 0.8703$$
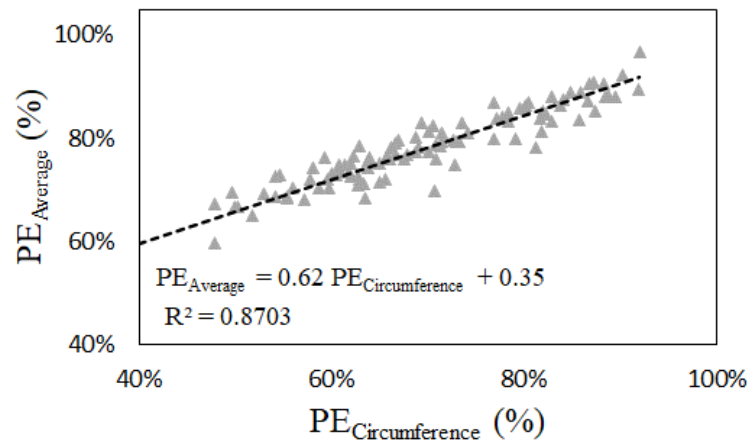
C. PE estimated using the average method versus circumference method

Figure 42. Plot. Scatterplots with regression lines of PE values estimated for Phase II sites.

Estimating PE from Texture Characteristics

With five texture parameters, including wavelet energies, and four PE estimation methods, the total number of possible basic models correlating PE to texture characteristics is 20. Additional models can be derived when separating the two test phases and incorporating the average least dimension as a model parameter. Out of the 80 possible combinations, the most reliable models were the ones correlating PE estimated using the each aggregate and average elevation methods with MPD calculated using the laser texture scanner and the side-view images.

Models Using Phase I Observations

Figure 43 and Figure 44 present the scatterplots and fitted regression lines for PE estimated using the average elevation method as a function of MPD estimated from laser texture scans and side-view images, respectively, for Phase I data. The figures show linear trends of decreasing PE values as MPD values increase. This decreasing trend matches the observation that lower PE values indicate more exposed aggregates and, accordingly, higher macrotexture peaks. Moreover, the regression lines

approach 100% PE value when MPD reaches 0, which corresponds to fully embedded aggregates that are not protruding from the surface. Note that the coefficient of determination (i.e., R^2) values shown in the figures, when multiplied by 100, indicate the percentage of the variance in PE that MPD explains. Accordingly, the low R^2 values can be attributed to the large variability in the observed PE for equal or similar MPD values and does not indicate that the model is insignificant. In fact, the models in Figure 43 and Figure 44 capture an observed engineering behavior and provide an unbiased trendline because the variability in observations is balanced around the line.
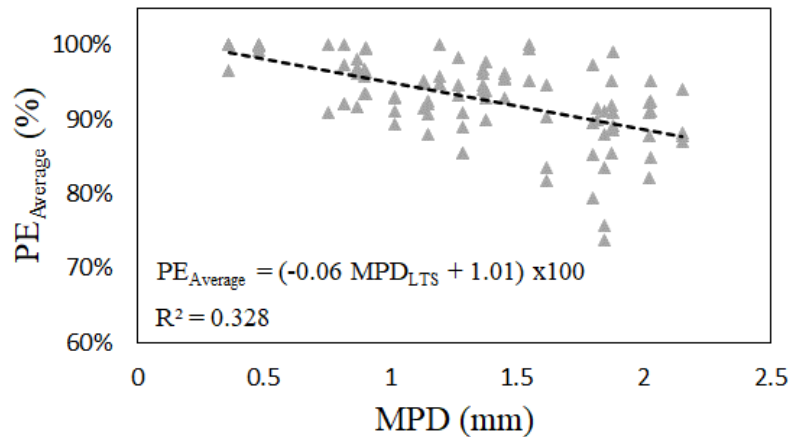
Figure 43. Plot. Percent embedment estimated using the average elevation method versus MPD calculated from LTS measurements for Phase I sites.
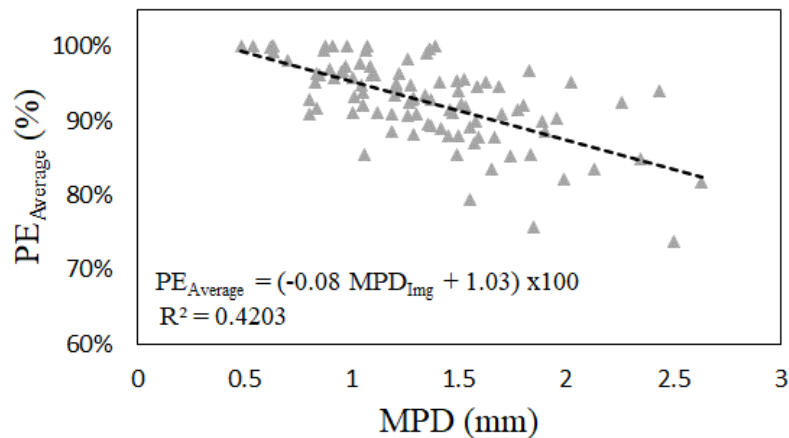
Figure 44. Plot. Percent embedment estimated using the average elevation method versus MPD calculated from side-view images for Phase I sites.

To explain more of the variability in the simple linear regression models, Table 8 and Table 9 present regression models developed to estimate PE values from MPD and the average least dimension (ALD) for Phase I data. As discussed in Chapter 4, ALD was estimated from the side-view images by transforming the pixel size to actual dimensions and measuring the vertical height of the aggregates in the top layer. Two multiple linear regression models were evaluated as described in Figure 45.

$$PE = (\beta_0 + \beta_1 MPD + \beta_2 ALD) \times 100\%$$

A. Model 1: PE as a function of MPD and ALD as two independent variables.

$$PE = (\beta_0 + \beta_1 MPD + \beta_2 ALD + \beta_3 MPD \times ALD) + 100\%$$

B. Model 2: PE as a function of MPD, ALD, and the interaction between them.

Figure 45. Equation. Multiple linear regression models relating PE to MPD and ALD.

Table 8 and Table 9 present an overall summary of the two models' statistics in the first segment of the tables. All models were statistically significant at 95% confidence level with an F-value less than 0.05. The adjusted R^2 values in the tables account for the additional number of variables in the regression models. This is important, because although additional variables can improve the model's accuracy during the fitting process, they will increase the model's sensitivity and variability in predictions. Accordingly, when selecting between multiple regression models, the one with higher adjusted R^2 value guarantees a better balance between robustness and accuracy, which is also known as the bias-variance tradeoff. The other two segments in Table 8 and Table 9 present a summary of the ANOVA analysis performed on the selected model and a summary of the model parameters. All selected model parameters are statistically significant and are greater than zero at a 95% confidence level. Model 2 using MPD from side-view images of Phase I test sites had a statistically insignificant model coefficient (β_2 coefficient for ALD). Therefore, Model 1 in Table 9 was selected over Model 2.

Table 8. Regression Model Outputs Correlating PE$_{average}$ with MPD$_{LTS}$ and ALD for Phase I Sites

Regression Statistics	Model 1 (Selected)	Model 2				
Multiple R	0.64	0.64				
R^2	0.40	0.40				
Adjusted R^2	0.39	0.38				
Standard Error	0.04	0.04				
Observations	98	98				
ANOVA (Model 1)						
	df	SS	MS	F	Significance F	
Regression	2	0.11	0.06	31.01	4.3E-11	
Residual	95	0.17	0.00			
Total	97	0.29				
Coefficients (Model 1)		Standard Error	t Stat	P-value	Lower 95%	Upper 95%
Intercept	0.94	0.03	37.48	< 0.05	0.89	0.99
MPD$_{LTS}$ (mm)	-0.06	0.01	-6.73	< 0.05	-0.08	-0.04
ALD (mm)	0.02	0.01	3.24	< 0.05	0.01	0.03

Table 9. Regression Model Outputs Correlating PE$_{average}$ with MPD$_{Img.}$ and ALD for Phase I Sites

Regression Statistics	Model 1 (Selected)	Model 2					
Multiple R	0.72	0.74					
R^2	0.52	0.55					
Adjusted R^2	0.51	0.53					
Standard Error	0.04	0.04					
Observations	0.72	98					
ANOVA (Model 1)							
	df	SS	MS	F	Significance F	
Regression	2	0.15	0.07	50.51	1.14E-15	
Residual	95	0.14	0.00			
Total	97	0.29				
Coefficients (Model 1)		Standard Error	t Stat	P-value	Lower 95%	Upper 95%
Intercept	0.95	0.02	43.24	< 0.05	0.91	1.00
MPD$_{Img}$ (mm)	-0.08	0.01	-8.95	< 0.05	-0.10	-0.06
ALD (mm)	0.03	0.01	4.32	< 0.05	0.01	0.04

Figure 46 and Figure 47 present the scatterplots and fitted regression lines for PE estimated using the each aggregate method as a function of MPD estimated from laser texture scans and side-view images, respectively, for Phase I data. The figures show a weak decreasing trend with low R^2 values.

$$PE_{Each\ Agg.} = (-0.02\ MPD_{LTS} + 0.84) \times 100$$
$$R^2 = 0.0163$$

Figure 46. Plot. Percent embedment estimated using the average PE values for individual aggregates versus MPD calculated from LTS measurements for Phase I sites.
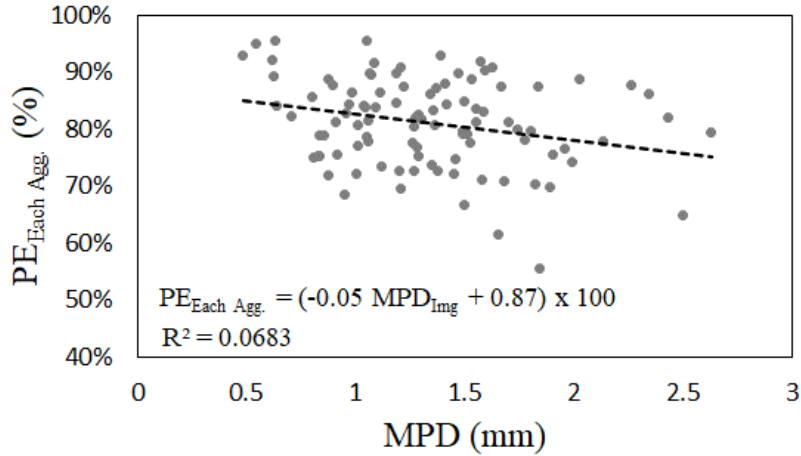
Figure 47. Plot. Percent embedment estimated using the average PE values for individual aggregates versus MPD calculated from side-view images for Phase I sites.

Table 10 presents the overall summary for additional regression models for PE estimated using the each aggregate method as a function of MPD from laser texture scanner and ALD. The selected model in the table indicates that the regression coefficient corresponding to MPD is statistically insignificant. Although the model is relatively weaker than previous models with an insignificant coefficient, it presents an improvement compared to the single variable model shown in Figure 46. Table 11 presents the overall summary for additional regression models for PE estimated using the each aggregate method as a function of MPD from side-view images and ALD. The selected model shows a significant improvement over the single-variable model and has significant regression coefficients.

Table 10. Regression Model Outputs Correlating PE_{Each} with MPD_{LTS} and ALD for Phase I Sites

Regression Statistics	Model 1 (Selected)	Model 2				
Multiple R	0.46	0.47				
R^2	0.22	0.22				
Adjusted R^2	0.20	0.20				
Standard Error	0.07	0.07				
Observations	0.46	98.00				
ANOVA (Model 1)						
	df	SS	MS	F	Significance F	
Regression	2	0.13	0.06	13.09	9.53E-06	
Residual	95	0.46	0.00			
Total	97	0.58				
Coefficients (Model 1)		Standard Error	t Stat	P-value	Lower 95%	Upper 95%
Intercept	0.66	0.04	16.29	< 0.05	0.58	0.75
MPD_{LTS} (mm)	-0.01	0.01	-0.79	0.43	-0.04	0.02
ALD (mm)	0.05	0.01	4.92	< 0.05	0.03	0.07

Table 11. Regression Model Outputs Correlating PE$_{Each}$ with MPD$_{Img.}$ and ALD for Phase I Sites

Regression Statistics	*Model 1 (Selected)*	*Model 2*				
Multiple R	0.52	0.53				
R^2	0.27	0.28				
Adjusted R^2	0.26	0.26				
Standard Error	0.07	0.07				
Observations	98	98				
ANOVA (Model 1)						
	df	*SS*	*MS*	*F*	*Significance F*	
Regression	2	0.16	0.08	17.78	2.75E-07	
Residual	95	0.43	0.00			
Total	97	0.58				
Coefficients (Model 1)		*Standard Error*	*t Stat*	*P-value*	*Lower 95%*	*Upper 95%*
Intercept	0.71	0.04	18.33	< 0.05	0.63	0.78
MPD$_{Img}$ (mm)	-0.04	0.02	-2.83	< 0.05	-0.07	-0.01
ALD (mm)	0.05	0.01	5.16	< 0.05	0.03	0.07

Models Using Phase II Observations

Figure 48 and Figure 49 present the scatterplots and fitted regression lines for PE estimated using the average elevation method as a function of MPD estimated from laser texture scans and side-view images, respectively, from Phase II. The figures show linear trends similar to the ones observed in Phase I data. The regression coefficients shown in Figure 48 and Figure 49 are similar to the ones observed in Figure 43 and Figure 44. This indicates that the trends using PE$_{Average}$ are consistent for both data sets. However, these plots and the corresponding regression models show greater variability in the data compared to Phase I data, which is exemplified in the lower R^2 values.
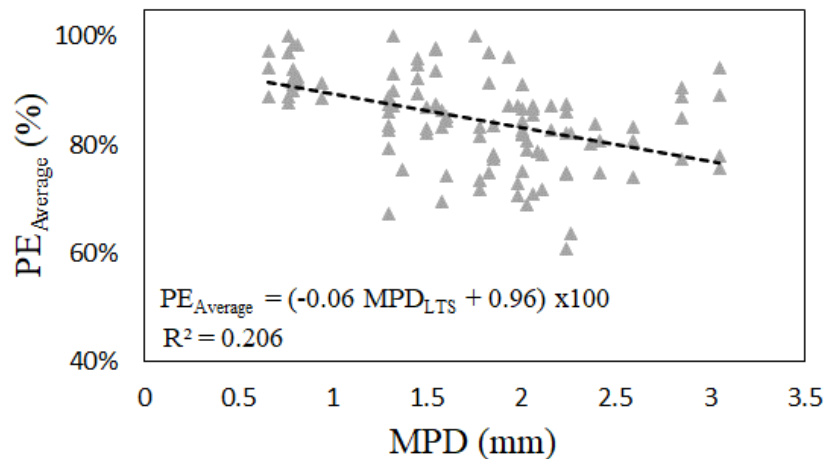
Figure 48. Plot. Percent embedment estimated using the average elevation method versus MPD calculated from LTS measurements for Phase II sites.
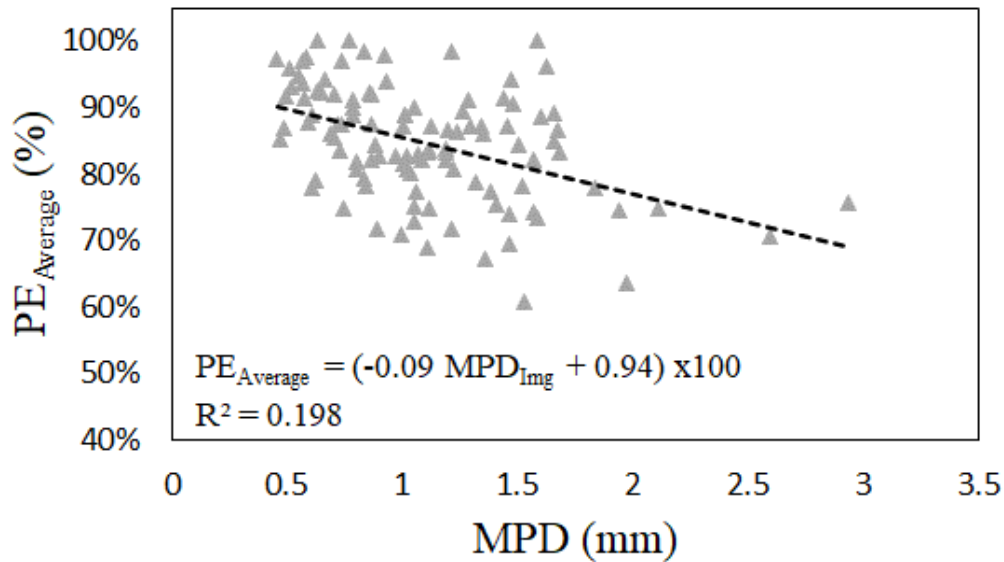
Figure 49. Plot. Percent embedment estimated using the average elevation method versus MPD calculated from side-view images for Phase II sites.

Table 12 and Table 13 show similar findings to Figure 48 and Figure 49. The models relating $PE_{average}$ for Phase II are similar to the models derived for Phase I data. However, the variability is also higher for Phase II data compared to Phase I data, which is exemplified in the lower R^2 values.

Table 12. Regression Model Outputs Correlating $PE_{average}$ with MPD_{LTS} and ALD for Phase II Sites

Regression Statistics	Model 1 (Selected)	Model 2				
Multiple R	0.51	0.51				
R^2	0.26	0.26				
Adjusted R^2	0.24	0.24				
Standard Error	0.07	0.07				
Observations	107	107				
ANOVA (Model 1)						
	df	SS	MS	F	Significance F	
Regression	2	0.20	0.10	18.04	1.89E-07	
Residual	104	0.57	0.01			
Total	106	0.77				
Coefficients (Model 1)		Standard Error	t Stat	P-value	Lower 95%	Upper 95%
Intercept	0.85	0.04	19.73	< 0.05	0.77	0.94
MPD_{LTS} (mm)	-0.06	0.01	-4.77	< 0.05	-0.08	-0.03
ALD (mm)	0.04	0.01	2.69	< 0.05	0.01	0.07

Table 13. Regression Model Outputs Correlating PE$_{average}$ with MPD$_{Img.}$ and ALD for Phase II Sites

Regression Statistics	Model 1 (Selected)	Model 2				
Multiple R	0.58	0.58				
R^2	0.33	0.33				
Adjusted R^2	0.32	0.31				
Standard Error	0.07	0.07				
Observations	107	107				
ANOVA (Model 1)						
	df	SS	MS	F	Significance F	
Regression	2	0.25	0.13	25.69	8.6E-10	
Residual	104	0.51	0.00			
Total	106	0.77				
Coefficients (Model 1)		Standard Error	t Stat	P-value	Lower 95%	Upper 95%
Intercept	0.80	0.03	23.18	< 0.05	0.74	0.87
MPD$_{Img}$ (mm)	-0.09	0.02	-6.05	< 0.05	-0.12	-0.06
ALD (mm)	0.06	0.01	4.54	< 0.05	0.04	0.09

Figure 50 and Figure 51 present the scatterplots and fitted regression lines for PE estimated using the each aggregate method as a function of MPD estimated from laser texture scans and side-view images, respectively, from Phase II. Figure 50 showed a stronger linear trend compared to Phase I data shown in Figure 46, with a significantly higher R^2 value. The correlation shown in Figure 51 developed using the image-based MPD for Phase II data is still weak with scattered observations and low R^2 value, which is similar to the observation from Phase I data in Figure 47.

$$PE_{Each\ Agg.} = (-0.11\ MPD_{LTS} + 0.88) \times 100$$
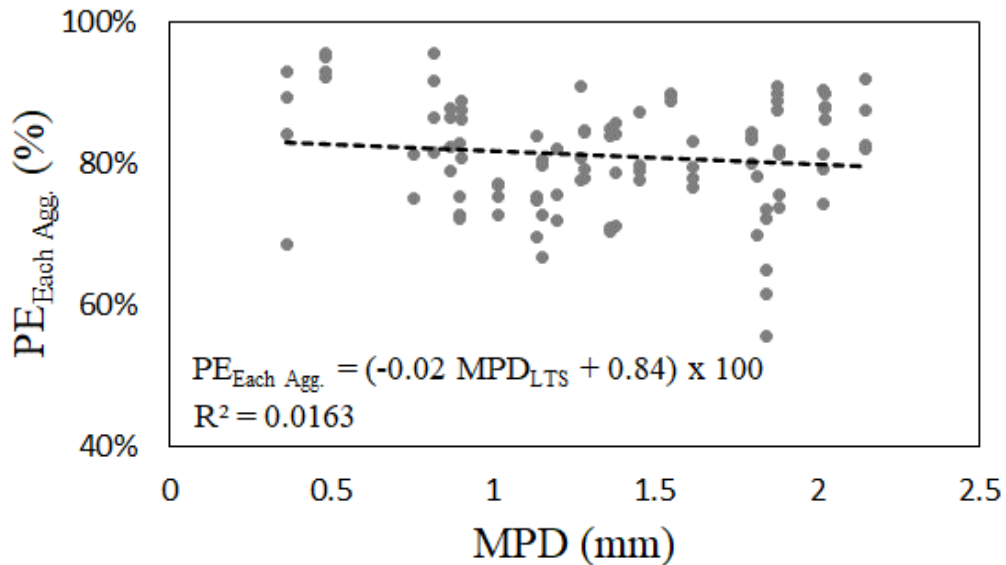$$R^2 = 0.3108$$
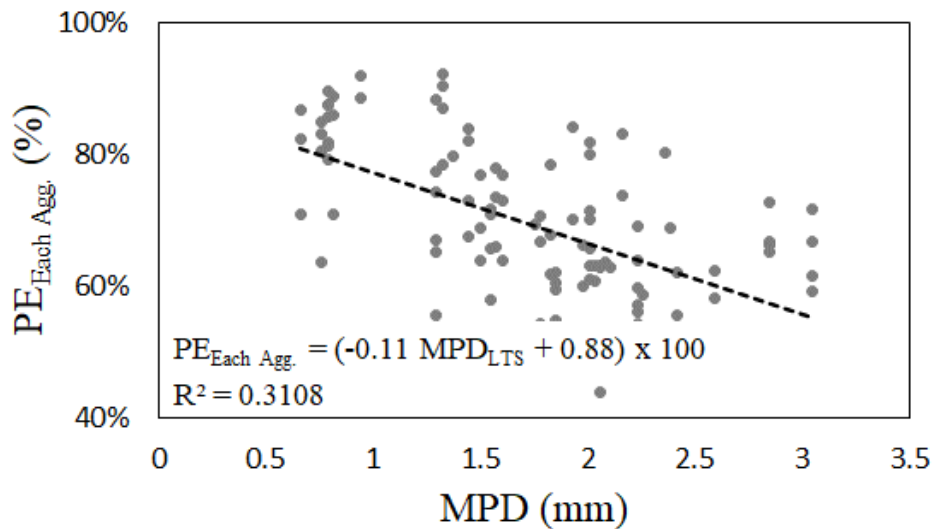
Figure 50. Plot. Percent embedment estimated using the average PE values for individual aggregates versus MPD calculated from LTS measurements for Phase II sites.

The equation shown in the plot:

$$PE_{Each\ Agg.} = (-0.08\ MPD_{Img} + 0.78) \times 100$$
$$R^2 = 0.0932$$
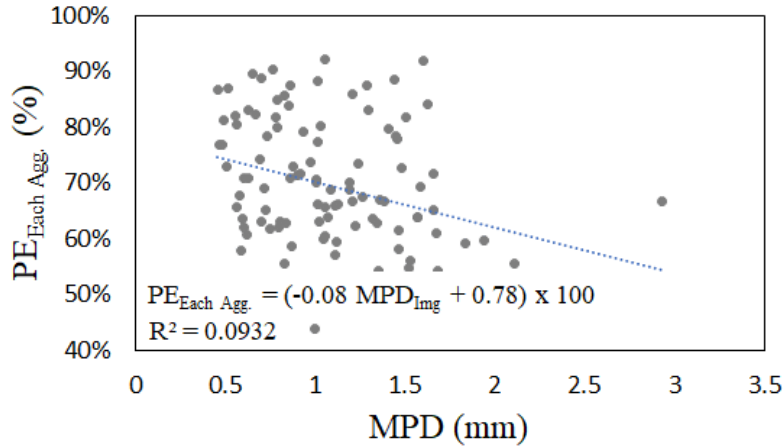
Figure 51. Plot. Percent embedment estimated using the average PE values for individual aggregates versus MPD calculated from side-view images for Phase II sites.

Similar to the observations made from Figure 50, Table 14 shows a significantly improved model compared to the model in Table 10 derived from Phase I data. Moreover, Model 1 was selected over Model 2 in Table 14 because the regression coefficients in Model 2 were all statistically insignificant except for the intercept. Table 15 presents the multiple linear regression models correlating PE estimated using the average of PE values measured for each aggregate to MPD and ALD estimated from the side-view images. The table shows that Model 1 yielded similar R^2 values with fewer regression variables compared to Model 2, and, therefore, it was selected.

Table 14. Regression Model Outputs Correlating PE$_{Each}$ with MPD$_{LTS}$ and ALD for Phase II Sites

Regression Statistics	Model 1 (Selected)	Model 2				
Multiple R	0.60	0.62				
R^2	0.36	0.38				
Adjusted R^2	0.35	0.37				
Standard Error	0.10	0.09				
Observations	107	107				
ANOVA (Model 1)						
	df	SS	MS	F	Significance F	
Regression	2	0.55	0.27	29.74	6.12E-11	
Residual	104	0.96	0.01			
Total	106	1.50				
Coefficients (Model 1)		Standard Error	t Stat	P-value	Lower 95%	Upper 95%
Intercept	0.74	0.06	13.11	< 0.05	0.62	0.85
MPD$_{LTS}$ (mm)	-0.10	0.02	-6.44	< 0.05	-0.13	-0.07
ALD (mm)	0.06	0.02	2.94	< 0.05	0.02	0.09

Table 15. Regression Model Outputs Correlating PE_{Each} with $MPD_{Img.}$ and ALD for Phase II Sites

Regression Statistics	Model 1 (Selected)	Model 2				
Multiple R	0.48	0.48				
R^2	0.23	0.23				
Adjusted R^2	0.22	0.21				
Standard Error	0.11	0.11				
Observations	107	107				
ANOVA (Model 1)						
	df	SS	MS	F	Significance F	
Regression	2	0.35	0.17	15.58	1.21E-06	
Residual	104	1.16	0.01			
Total	106	1.50				
Coefficients (Model 1)		Standard Error	t Stat	P-value	Lower 95%	Upper 95%
Intercept	0.59	0.05	11.32	< 0.05	0.49	0.69
MPD_{Img} (mm)	-0.09	0.02	-4.04	< 0.05	-0.14	-0.05
ALD (mm)	0.09	0.02	4.31	< 0.05	0.05	0.13

In summary, regression models for PE values estimated using the average elevation method were consistent for Phase I and Phase II data. The models have shown a consistent decreasing trend between PE and MPD estimated using laser texture scans and side-view images. Moreover, the models for PE estimated using the average elevation method matched the expected behavior that PE should reach 100% as MPD reaches 0. This physical interpretability is very important when selecting the appropriate empirical models and definitions.

In addition to the simple linear models, multiple linear regression models—adding the estimated ALD as a model variable—significantly improve model performance and predictive power. Similar to the conclusions from the simple linear regression models, the models derived for PE estimated using the average elevation method outperformed the models developed for PE estimated using the average of PE values measured for each aggregate. Moreover, Model 1 including MPD and ALD as the regression variables were always selected over Model 2, which includes an additional interaction variable.

General Models for Phase I and Phase II Data

To derive a general regression model, data from Phases I and II were combined and analyzed. In addition to combining the data from both phases, PE values, ALD, and MPD estimated from the side-view images were averaged for each core. This represents more realistic results, because it averages the results from all sides of the same core. Figure 52 and Figure 53 present the scatterplots and fitted regression lines for PE estimated using the average elevation method as a function of MPD estimated from laser texture scans and side-view images, respectively, for the combined and averaged data. The figures show a linear trend similar to the ones observed in Phase I and Phase II data. Using the laser texture scanner to estimate MPD yields more consistent data with lower variability and higher R^2

values, as shown in Figure 52. Moreover, the R^2 value in Figure 52 is significantly higher than the individual values shown in Figure 43 and Figure 48. On the contrary, Figure 53 shows a significantly lower R^2 value compared to the individual values shown in Figure 44 and Figure 49. This indicates that the trendline fitted for Phase I data are different than the trendlines fitted for Phase II data due to the inconsistent MPD values estimated from side-view images.
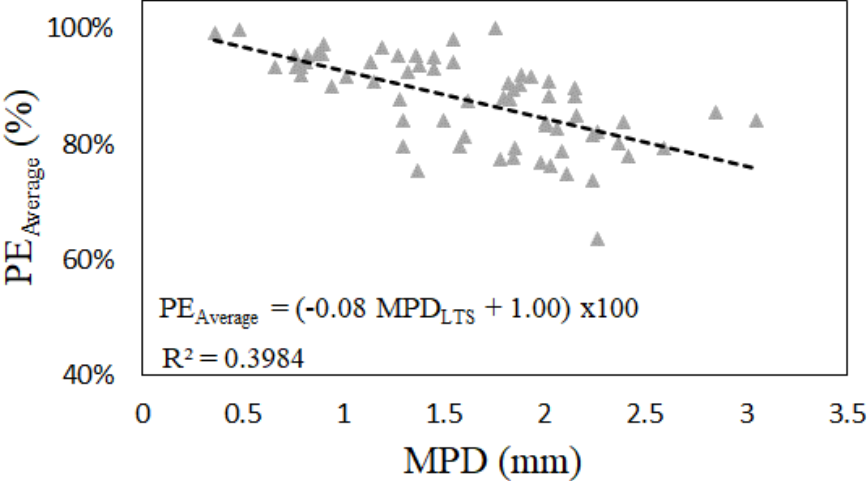
Figure 52. Plot. Percent embedment estimated using the average elevation method versus MPD calculated from LTS measurements for Phases I and II sites.
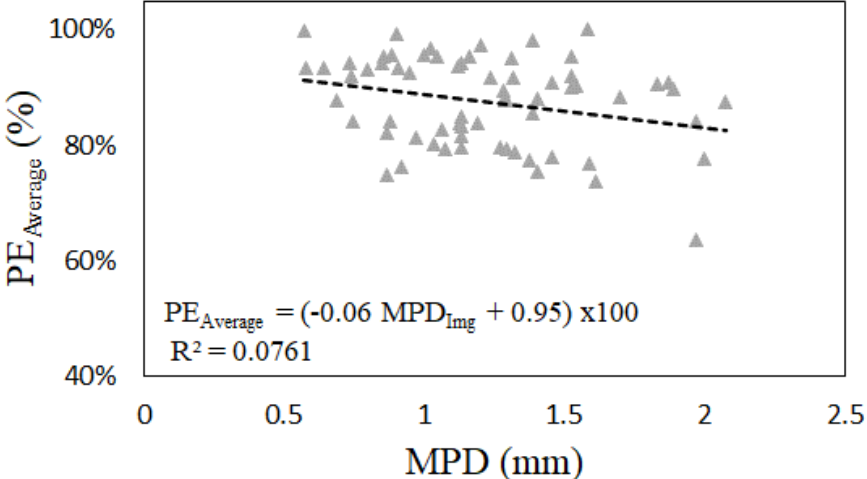
Figure 53. Plot. Percent embedment estimated using the average elevation method versus MPD calculated from side-view images for Phases I and II sites.

Table 16 and Table 17 present a summary of the regression models derived from the combined and averaged data collected in Phases I and II. All models were statistically significant at 95% confidence level with an F-value less than 0.05. The tables show significant increase in the R^2 compared to the simple regression models presented in Figure 52 and Figure 53. Model 1 with two regression variables was selected because the addition of the interaction term reduced the adjusted R^2 values.

Moreover, Model 2 derived using the image-based MPD in Table 17 yielded statistically insignificant regression coefficients except for the intercept.

Table 16. General Regression Model Outputs Correlating PE$_{average}$ with MPD$_{LTS}$ and ALD

Regression Statistics	Model 1 (Selected)	Model 2				
Multiple R	0.72	0.72				
R^2	0.51	0.52				
Adjusted R^2	0.50	0.49				
Standard Error	0.05	0.05				
Observations	66	66				
ANOVA (Model 1)						
	df	SS	MS	F	Significance F	
Regression	2	0.20	0.10	33.10	1.5E-10	
Residual	63	0.19	0.00			
Total	65	0.39				
Coefficients (Model 1)		Standard Error	t Stat	P-value	Lower 95%	Upper 95%
Intercept	0.86	0.04	19.51	< 0.05	0.77	0.95
MPD$_{LTS}$ (mm)	-0.06	0.01	-4.92	< 0.05	-0.09	-0.04
ALD (mm)	0.05	0.01	3.84	< 0.05	0.02	0.07

Table 17. General Regression Model Outputs Correlating PE$_{average}$ with MPD$_{Img.}$ and ALD

Regression Statistics	Model 1 (Selected)	Model 2				
Multiple R	0.67	0.67				
R^2	0.45	0.45				
Adjusted R^2	0.43	0.43				
Standard Error	0.06	0.06				
Observations	66	66				
ANOVA (Model 1)						
	df	SS	MS	F	Significance F	
Regression	2	0.17	0.09	25.95	6.02E-09	
Residual	63	0.21	0.00			
Total	65	0.39				
Coefficients (Model 1)		Standard Error	t Stat	P-value	Lower 95%	Upper 95%
Intercept	0.77	0.04	21.12	< 0.05	0.70	0.84
MPD$_{Img}$ (mm)	-0.08	0.02	-3.81	< 0.05	-0.11	-0.04
ALD (mm)	0.08	0.01	6.57	< 0.05	0.05	0.10

Figure 54 and Figure 55 present the scatterplots and fitted regression lines for PE estimated using each aggregate method as a function of MPD estimated from laser texture scans and the side-view images, respectively, for the combined and averaged data. Figure 54 shows a stronger linear trend compared to Phase I and Phase II data shown in Figure 46 and Figure 50, with a significantly higher R^2 value. The correlation shown in Figure 55 developed using the image-based MPD is weak with scattered observations and low R^2 value, which is similar to the observation from Phase I and Phase II.
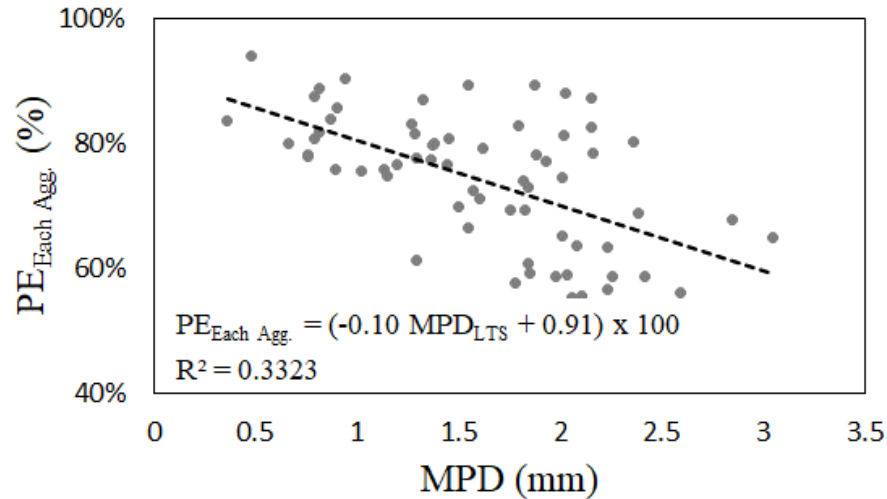
Figure 54. Plot. Percent embedment estimated using the average PE values for individual aggregates versus MPD calculated from LTS measurements for Phases I and II sites.
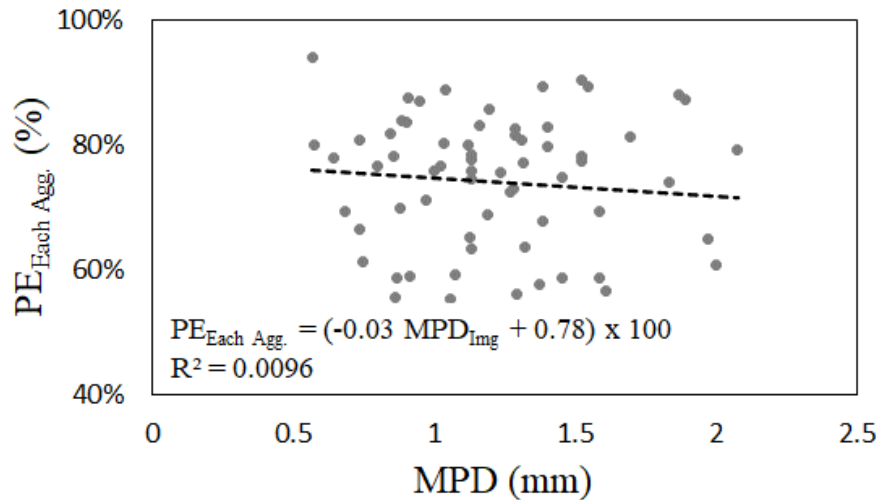
Figure 55. Plot. Percent embedment estimated using the average PE values for individual aggregates versus MPD calculated from side-view images for Phases I and II sites.

Table 18 and Table 19 present a summary of the regression models derived using combined and averaged data collected in Phases I and II. All models were statistically significant at 95% confidence level with an F-value less than 0.05. The tables show significant increase in the R^2 compared to the simple regression models presented in Figure 54 and Figure 55. Model 1 with two regression

variables was selected because the addition of the interaction term reduced the adjusted R^2 values. Moreover, Model 2 derived using the image-based MPD in Table 19 yielded statistically insignificant regression coefficients except for the intercept.

Table 18. General Regression Model Outputs Correlating PE$_{Each}$ with MPD$_{LTS}$ and ALD

Regression Statistics	Model 1 (Selected)	Model 2				
Multiple R	0.66	0.66				
R^2	0.43	0.43				
Adjusted R^2	0.41	0.41				
Standard Error	0.08	0.08				
Observations	66	66				
ANOVA (Model 1)						
	df	SS	MS	F	Significance F	
Regression	2	0.32	0.16	23.90	1.89E-08	
Residual	63	0.42	0.01			
Total	65	0.74				
Coefficients (Model 1)		Standard Error	t Stat	P-value	Lower 95%	Upper 95%
Intercept	0.71	0.07	10.85	< 0.05	0.58	0.85
MPD$_{LTS}$ (mm)	-0.08	0.02	-4.13	< 0.05	-0.12	-0.04
ALD (mm)	0.06	0.02	3.31	< 0.05	0.02	0.10

Table 19. General Regression Model Outputs Correlating PE$_{Each}$ with MPD$_{Img.}$ and ALD

Regression Statistics	Model 1 (Selected)	Model 2				
Multiple R	0.55	0.56				
R^2	0.31	0.31				
Adjusted R^2	0.28	0.27				
Standard Error	0.09	0.09				
Observations	66	66				
ANOVA (Model 1)						
	df	SS	MS	F	Significance F	
Regression	2	0.23	0.11	13.92	9.86E-06	
Residual	63	0.52	0.01			
Total	65	0.74				
Coefficients		Standard Error	t Stat	P-value	Lower 95%	Upper 95%
Intercept	0.56	0.06	9.82	< 0.05	0.45	0.67
MPD$_{Img}$ (mm)	-0.05	0.03	-1.62	< 0.05	-0.11	0.01
ALD (mm)	0.09	0.02	5.19	< 0.05	0.06	0.13

In summary, the general regression models for PE values estimated using the average elevation method and MPD acquired using laser texture scans yielded the highest R^2 value. The next most reliable general regression models are the ones for PE values estimated using the each aggregate method and the MPD acquired using laser texture scans. The models have shown a consistent decreasing trend between PE and MPD estimated using laser texture scans and side-view images. Moreover, the models for PE estimated using the average elevation method matched the expected behavior that PE should reach 100% as MPD reaches 0. Accordingly, Figure 56 presents the recommended models relating PE estimated using the average elevation method to MPD (mm) estimated from laser texture scans and ALD (mm) estimated from side-view images. Alternatively, Figure 57 presents the recommended models relating PE estimated using the each aggregate method to MPD (mm) estimated from laser texture scans and ALD (mm) estimated from side-view images. Note that the ALD values may vary slightly if estimated using laboratory procedures on a sample of aggregates.

$$PE_{Average} = (1.00 - 0.08\,MPD_{LTS}) \times 100\%;\quad R^2 = 0.40$$

A. General regression model representing PE$_{Average}$ as a function of MPD$_{LTS}$

$$PE_{Average} = (0.86 - 0.06\,MPD_{LTS} + 0.05\,ALD) \times 100\%;\quad R^2 = 0.50$$

B. General regression model representing PE$_{Average}$ as a function of MPD$_{LTS}$ and ALD

Figure 56. Equation. General regression models representing PE estimated using the average elevation method as a function of MPD estimated from laser texture scans and ALD.

$$PE_{Each} = (0.91 - 0.1\,MPD_{LTS}) \times 100\%;\quad R^2 = 0.33$$

A. General regression model representing PE$_{Each}$ as a function of MPD$_{LTS}$

$$PE_{Each} = (0.71 - 0.08\,MPD_{LTS} + 0.06\,ALD) \times 100\%;\quad R^2 = 0.41$$

B. General regression model representing PE$_{Each}$ as a function of MPD$_{LTS}$ and ALD

Figure 57. Equation. General regression models representing PE estimated using the each aggregate method as a function of MPD estimated from laser texture scans and ALD.

Estimating PE from Overhead Image-Texture Analysis

As discussed in Chapter 4, PE for individual aggregates was estimated by calculating the height of exposed aggregates from the surrounding binder and then back-calculating the PE using an ALD. The exposed aggregate height was validated by investigating individual texture scans. Figure 58 presents the scatterplots and regression lines correlating the PE values estimated using the average elevation method and the each aggregate method from side-view images to the average PE values from the overhead measurements. The plots show a positive linear trend with high scatter around the regression line. This high variability can be attributed to the inaccurate assumption of a uniform ALD for all aggregates in each core. The data and analysis procedures are promising but require additional validation and more accurate evaluation of ALD values.
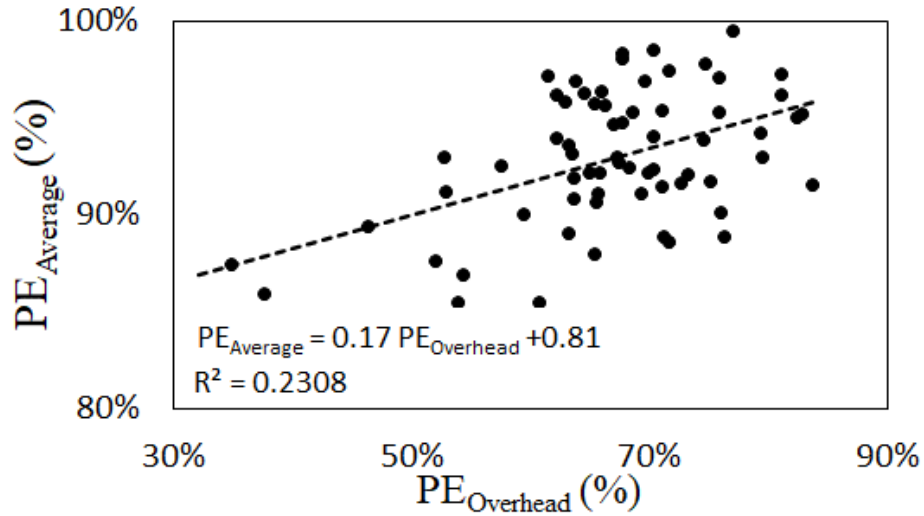
A. A scatterplot with a regression line correlating the PE values estimated using the average elevation method from side-view images and the average PE values from overhead measurements.
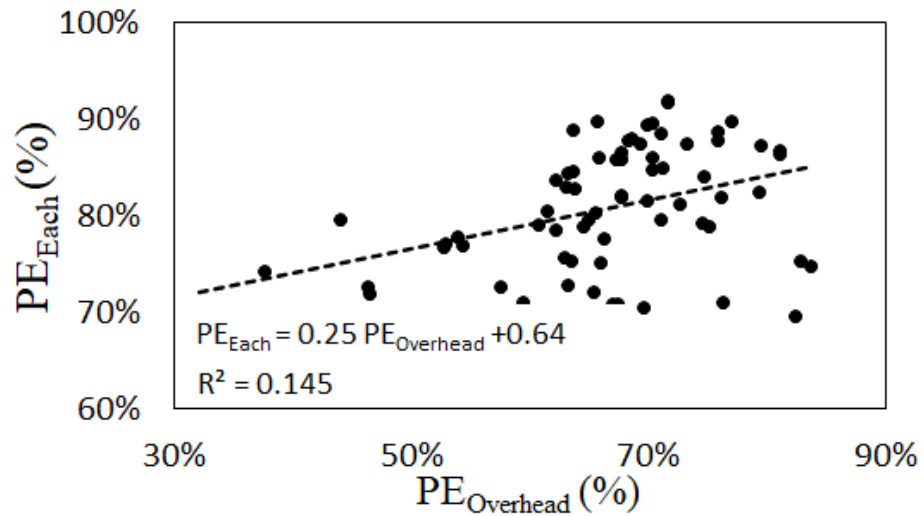
B. A scatterplot with a regression line correlating the PE values estimated using the each aggregate method from side-view images and the average PE values from overhead measurements.

Figure 58. Plot. Scatterplots with regression lines correlating the PE values estimated using the average elevation method and each aggregate method from side-view images to the average PE values from overhead measurements.

CHAPTER 6: RECOMMENDATIONS AND CONCLUSIONS

SUMMARY

Chip seal application is a common maintenance and preservation treatment for deteriorated pavements. This application is used mainly to seal fine cracks on a pavement surface and to prevent water intrusion into the pavement foundation, thereby extending the life span of the existing pavement. In addition, chip seals are also frequently used to restore surface texture and friction in an effort to improve some skid-resistant characteristics and to improve roadway safety.

In general, chip seal applications involve spraying or spreading a layer of asphalt binder or emulsion followed by a layer of aggregates (chips). These chips are embedded and reoriented in the binder by passing a roller over the newly spread aggregate layer. As such, the performance of chip seals depends on percent embedment, which is defined as the ratio between the height of the asphalt binder (i.e., the depth of aggregate embedment) and the height of the aggregate. The target embedment should be within a controlled range, typically between 50% and 70%. Higher embedment can lead to higher bleeding/flushing potential, while lower embedment can lead to aggregate loss and raveling.

Although quality assurance is important for all paving and treatment projects, there is no agreement on well-established quantitative procedures and QA programs for chip seal practices in the literature. State highway agencies may have different procedures for simplified QA measurements of chip seals. One of the practices is to estimate PE by pulling some of the chips after construction and visually examining the PE values. This practice does not guarantee representative samples and lacks consistency and objectivity because there are no specifications on how to measure PE from retrieved aggregates. The macrotexture of a chip seal surface may provide a close relationship to the percent embedment of aggregates. As such, several studies have proposed to use macrotexture as an indicator of the percent embedment and, subsequently, as a QA tool for chip seals. However, the effectiveness of these macrotexture measurements for QA of chip seals is not well established, especially under field conditions.

The primary objective of this study is to investigate the relationship between surface macrotexture and the percent embedment (PE) of chip seals under different field conditions. More specifically, the objectives of this study are listed as follows:

- Determine if texture measurements can be used to calculate the percent embedment accurately.

- Identify the appropriate surface texture measurement as well as other parameters to be correlated with percent embedment.

- Identify an accurate and cost-effective method for chip seal texture measurement using the best available technology.

Two testing phases were performed in 2021 and 2022 to investigate the relationship between surface texture and PE. The field-testing program in 2021 included 10 in-service chip seal sections in Illinois. In 2022, a construction project on a road segment along Illinois Route 116 near Roseville included

nine unique test sections with varying materials and construction methods. In addition to the construction project sections, five in-service sections were also tested to further validate the test procedures. Including the sites tested in 2021 and 2022, the study involved 24 test sections. The test sites covered a wide range of treatment ages and locations to capture different traffic volumes, materials used in these locations, and construction practices such as binder and chip application rate.

At each site, the tests were performed within 152 m (500 ft) test sections marked using reflective tape at the beginning and end of the section. The field tests included high-speed texture profiles acquired on the left and right wheel paths. Three repetitions of the high-speed texture profiles were conducted at 56 kmh (35 mph) for each site. Following the high-speed texture profiles, handheld stationary laser texture scans were acquired at 15, 76, and 137 m (50, 250, and 450 ft), measured from the beginning of the test sections. Finally, cores were extracted at the handheld scanning locations in the right wheel path for additional texture scans, cross section image acquisition, and overhead image analysis.

Based on the evaluation performed in this study, the surface texture acquired using the high-speed texture profiler provided continuous texture measurements across the entire test site. However, the estimated texture parameters using the high-speed texture profiler were not always consistent and reliable. Accordingly, high-speed texture measurements are not recommended at this stage for estimating PE values. The stationary laser texture scanner provided more consistent and reliable texture measurements and showed significant correlations to the estimated PE values.

To characterize the chip seal surface texture, the following parameters were calculated for individual lines in the stationary texture scans: mean profile depth (MPD), arithmetic mean deviation (Ra), root mean square (RMS), skewness (Rsk), and wavelet energy and power spectral density (PSD). Based on the performed analysis, MPD provided sufficient information for estimating PE values. In addition, PSD provided more detailed information that can be used to compare different laser texture measurement devices and tools.

The acquired cores were trimmed, and images were acquired from the four sides of the trimmed cores to estimate the ground truth PE values using in-house image-analysis algorithms. In addition to estimating PE values, side-view images were used to estimate surface texture and the average least dimension (ALD) of the aggregates. The ground truth PE values were estimated using four approaches: average elevation method, percent embedment of each aggregate method, peak method, and aggregate circumference method.

The analysis showed that the correlations are relatively weak between the different PE estimation methods. This finding indicates that the methods provide different information and may relate to different characteristics. Note that although the overall trends were consistent between Phase I and Phase II data, the regression equations were significantly different for the same regression variables. That variability can be attributed to the different construction practices and the fact that cores acquired in Phase II had emulsion smeared over some aggregates, which has a major impact on PE estimations.

To investigate the relationship between PE and surface texture measurements, simple and multiple linear regression models were developed using the PE values estimated using various methods and texture parameters. With five texture parameters, including wavelet energies, and four PE estimation

methods, the total number of possible basic models correlating PE to texture characteristics is 20. Additional models can be derived when separating the two test phases and incorporating the average least dimension as a model parameter. Out of the 80 possible combinations, the most reliable models correlated PE estimated using the each aggregate and average elevation methods with MPD calculated using the laser texture scanner and side-view images.

In summary, regression models for PE values estimated using the average elevation method were consistent for Phase I and Phase II data. The models showed a consistent decreasing trend between PE and MPD estimated using laser texture scans and side-view images. Moreover, the models for PE estimated using the average elevation method matched the expected behavior that PE should reach 100% as MPD reaches zero. This physical interpretability is very important when selecting the appropriate empirical models and definitions.

In addition to the simple linear models, two possible multiple linear regression models were evaluated. The first set of multiple linear regression models were developed by adding ALD in addition to MPD as a regression variable. The second set of multiple linear regression models included ALD and the interaction between MPD and ALD as a third regression variable. Adding the estimated ALD as a variable significantly improved the model's performance and predictive power. Similar to the conclusions from the simple linear regression models, the models derived for PE estimated using the average elevation method outperformed the models developed for PE estimated using the average of PE values measured for each aggregate. Moreover, the models including MPD and ALD as regression variables were always selected over the models including the interaction variable.

To derive a general regression model, data from Phases I and II were combined and analyzed. In addition, PE values, ALD, and MPD estimated from side-view images were averaged for each core. This represents more realistic results because it averages the results from all sides of the same core.

The general regression models for PE values estimated using the average elevation method and MPD acquired using laser texture scans yielded the highest R^2 value. The next most reliable general regression models are the ones for PE values estimated using the average elevation method and the MPD acquired using laser texture scans. The models showed a consistent decreasing trend between PE and MPD estimated using the laser texture scans and side-view images.

To overcome the need for coring in the field, a prototype frame was designed and built to acquire laser texture scans and overhead images of chip seal surfaces in the field or in a controlled environment using cores. An analysis procedure and algorithms were developed to process the acquired overhead texture scans and images. This procedure estimates the exposed aggregate heights accurately and then estimates the PE values assuming the ALD of these aggregates. The estimation of the exposed aggregates is consistent and accurate; however, the estimated PE will require more accurate ALD measurements and will be mostly applicable for chip seals constructed with a single aggregate size.

RECOMMENDATIONS

- To characterize the surface texture for a test segment, it is recommended to acquire a minimum of one stationary texture measurement every 60 m (~200 ft) in the field, with a

minimum of three texture scans for each construction site. Additional texture scans may be required if high variability is observed in the test section. At each texture scan location, it is recommended to acquire a minimum of 100 scan lines for a scan width of 71.61 × 101.60 mm (2.82 × 4.00 in.). The recommended maximum point spacing in each line is 7.94 × 10^{-3} mm (3.13 × 10^{-3} in.). For larger projects, longer than 1.61 km (1 mile), there should be a 305 m (1,000 ft) test segment where data is collected in detail, as described above. Beyond the test segment, the spacing between the stationary scans can be increased, or replaced with high-speed texture scans if reliable in the future.

- Figure 59 presents the recommended models relating PE estimated using the average elevation method to the MPD (mm) estimated from laser texture scans and ALD (mm) estimated from side-view images. Alternatively, Figure 60 presents the recommended models relating PE estimated using the each aggregate method to the MPD (mm) estimated from laser texture scans and ALD (mm) estimated from side-view images.

- It is recommended to use the models relating PE estimated using the average elevation method for in-service sections. Alternatively, models relating PE estimated using the each aggregate method is recommended for newly constructed projects.

- The correlations using ALD should be updated and revised once the data is available for ALD values measured using laboratory procedures on a sample of aggregates.

$$PE_{Average} = (1.00 - 0.08\ MPD_{LTS}) \times 100\%;\quad R^2 = 0.40$$

A. General regression model representing PE$_{Average}$ as a function of MPD$_{LTS}$

$$PE_{Average} = (0.86 - 0.06\ MPD_{LTS} + 0.05\ ALD) \times 100\%;\quad R^2 = 0.50$$

B. General regression model representing PE$_{Average}$ as a function of MPD$_{LTS}$ and ALD

Figure 59. Equation. General regression models representing PE estimated using the average elevation method as a function of MPD estimated from laser texture scans and ALD.

$$PE_{Each} = (0.91 - 0.1\ MPD_{LTS}) \times 100\%;\quad R^2 = 0.33$$

A. General regression model representing PE$_{Each}$ as a function of MPD$_{LTS}$

$$PE_{Each} = (0.71 - 0.08\ MPD_{LTS} + 0.06\ ALD) \times 100\%;\quad R^2 = 0.41$$

B. General regression model representing PE$_{Each}$ as a function of MPD$_{LTS}$ and ALD

Figure 60. Equation. General regression models representing PE estimated using the each aggregate method as a function of MPD estimated from laser texture scans and ALD.

- The use of overhead texture scanning and imaging setup is promising. It is recommended to explore additional improvements and refinements to the system.

REFERENCES

AASHTO R10. (2020). *Standard practice for definition of terms related to quality and statistics as used in highway construction*. American Association of State and Highway Transportation Officials.

AASHTO M 247-13. (2022). *Standard specification for glass beads used in pavement markings*. American Association of State and Highway Transportation Officials.

Adams, J., Castorena, C., & Kim, Y. R. (2019). Construction quality acceptance performance-related specifications for chip seals. *Journal of Traffic and Transportation Engineering (English Edition)*, *6*(4), 337–348. https://doi.org/10.1016/j.jtte.2019.05.003

Adams, J. M., & Richard Kim, Y. (2014). Mean profile depth analysis of field and laboratory traffic-loaded chip seal surface treatments. *International Journal of Pavement Engineering*, *15*(7), 645–656. https://doi.org/10.1080/10298436.2013.851790

Alhasan, A., Smadi, O., Walton, R., & Schleppi, B. L. (2020). Pavement texture characterisation using wavelets analysis in relation to pendulum skid tester. *International Journal of Pavement Engineering*, *22*(3), 2320–2334. https://doi.org/10.1080/10298436.2020.1852562

ASTM E1845-15. (2015). *Standard practice for calculating pavement macrotexture mean profile depth*. ASTM International. https://doi.org/10.1520/E1845-15

ASTM E965-15. (2019). *Standard test method for measuring pavement macrotexture depth using a volumetric technique*. ASTM International. https://doi.org/10.1520/E0965-15R19.

Boz, I., Kumbargeri, Y., Kutay, M. E., & Haider, S. W. (2018). *Establishing percent embedment limits to improve chip seal performance* (Report No. SPR-1679). Michigan Department of Transportation.

Boz, I., Kumbargeri, Y. S., & Kutay, M. E. (2019). Performance-based percent embedment limits for chip seals. *Transportation Research Record*, *2673*(1), 182–192. https://doi.org/10.1177/0361198118821370

Chamberlin, W. P., & Amsler, D. E. (1982). Measuring surface texture by the sand-patch method. *Pavement surface characteristics and materials*, https://doi.org/10.1520/STP28459S

Dumas, B. (2001). The determination of the average least dimension of surfacing aggregates by computation. *SATC 2001*, SATC.

Epps, J. A., Chaffin, C. W., & Hill, A. J. (1980). *Field evaluation of a seal coat design method* (Report No. 214-23). Texas Transportation Institute.

Epps, J. A., & Gallaway, B. M. (1972). *Synthetic aggregate seal coats—Current Texas Highway Department practices* (Report No. 83-1). Texas Transportation Institute.

Federal Highway Administration. (2017). *Pavement Preservation Checklist Series 2: Chip Seal*. Federal Highway Administration. https://www.fhwa.dot.gov/pavement/preservation/ppcl02.pdf

Gransberg, D. D., & James, D. M. B. (2005). *Chip seal best practices* (NCHRP Synthesis 342). National Cooperative Highway Research Program.

Haider, S. W., Boz, I., Kumbargeri, Y., Kutay, E., & Musunuru, G. (2021). Development of performance

related specifications for chip seal treatments. *International Journal of Pavement Engineering*, *22*(3), 382–391. https://doi.org/10.1080/10298436.2019.1610173

Illinois Department of Transportation. (2017). *Seal Coats (Oil & Chipping)*. Illinois Department of Transportation, Bureau of Local Roads and Streets.

ISO/TS 13473-4. (2008). *Characterization of pavement texture by use of surface profiles—Part 4: Spectral analysis of surface profiles*.

Jeong, J., Adams, J. M., & Richard Kim, Y. (2020). Chip seal construction variability and its impact on performance. *Journal of Transportation Engineering, Part B: Pavements*, *146*(4), 4020059. https://doi.org/10.1061/JPEODX.0000218

Kearby, J. P. (1953). Tests and theories on penetration surfaces. *Highway Research Board Proceedings*.

Kim, Y. R., & Adams, J. (2011). *Development of a new chip seal mix design method* (Report No. HWY-2008-04). North Carolina Department of Transportation.

Kim, Y. R., Adams, J., & Jeong, J. (2018). *Chip seal construction variability and its impact on performance* (Report No. HWY-2015-19). North Carolina Department of Transportation.

Kim, Y. R., & Im, J. H. (2014). *Extending the use of chip seals to high volume roads by using polymer-modified emulsions and optimized construction procedures* (Report No. HWY-2011-03). North Carolina Department of Transportation.

Kirillov, A., Mintun, E., Ravi, N., Mao, H., Rolland, C., Gustafson, L., Xiao, T., Whitehead, S., Berg, A. C., & Lo, W.-Y. (2023). Segment anything. *arXiv preprint arXiv:2304.02643*.

Kumbargeri, Y., Boz, I., & Kutay, M. E. (2021). Comparative investigation of hot-applied and emulsion-based chip seal treatments using image processing techniques and performance tests. *Journal of Transportation Engineering, Part B: Pavements*, *147*(3), 4021039. https://doi.org/10.1061/JPEODX.0000278

Kumbargeri, Y. S., Boz, I., & Kutay, M. E. (2019). Investigating the effect of binder and aggregate application rates on performance of chip seals via digital image processing and sweep tests. *Construction and Building Materials*, *222*, 213–221. https://doi.org/10.1016/j.conbuildmat.2019.06.089

Kumbargeri, Y. S., Kutay, M. E., & Boz, I. (2018). Effect of percent embedment on chip seal performance using FE modeling. In E. Masad, A. Bhasin, T. Scarpas, I. Menapace, & A. Kumar (Eds.), *Advances in Materials and Pavement Performance Prediction* (pg. 583–586). CRC Press.

Kutay, M. E., & Ozdemir, U. (2016). *An acceptance test for chip seal projects based on image analysis.* Michigan State University. Center for Highway Pavement Preservation.

Kutay, M. E., Ozdemir, U., Hibner, D., Kubargeri, Y., & Lanotte, M. (2016). *Development of an acceptance test for chip seal projects*. Michigan State University.

Lee, J., & Kim, Y. R. (2010). Evaluation of performance and cost-effectiveness of polymer-modified chip seals. *Transportation Research Record*, *2150*(1), 79–86. https://doi.org/10.3141/2150-10

Lee, J., Kim, Y. R., & McGraw, E. O. (2006). Performance evaluation of bituminous surface treatment

using third-scale model mobile loading simulator. *Transportation Research Record*, *1958*(1), 59–70. https://doi.org/10.1177/0361198106195800107

McGhee, K. K., & Flintsch, G. W. (2003). *High-speed texture measurement of pavements* (Report No. VTRC 03-R9). Virginia Center for Transportation Innovation and Research.

McHattie, R. L. (2001). *Asphalt surface treatment guide* (Report No. FHWA-AK-RD-01-03). Alaska Department of Transportation and Public Facilities.

McLeod, N. W. (1969). A general method of design for seal coats and surface treatments. *Proceedings of the Association of Asphalt Paving Technologists*, *38*(1), 537–630.

Ozdemir, U., Kutay, M. E., Hibner, D., Lanotte, M., & Kumbargeri, Y. S. (2018). Quantification of aggregate embedment in chip seals using image processing. *Journal of Transportation Engineering, Part B: Pavements*, *144*(4), 4018047. https://doi.org/10.1061/JPEODX.0000068

Pourhassan, A., Gheni, A. A., & ElGawady, M. A. (2023). Raveling performance of conventional and rubberized chip seal under field and laboratory traffic loading. *Construction and Building Materials*, *370*, 130674. https://doi.org/10.1016/j.conbuildmat.2023.130674

Seitllari, A., & Kutay, M. E. (2018). Soft computing tools to predict progression of percent embedment of aggregates in chip seals. *Transportation Research Record*, *2672*(12), 32–39. https://doi.org/10.1177/0361198118756868

Shuler, S., Lord, L., Epps-Martin, A., & Hoyt., D. (2005). *Manual for emulsion-based chip seals for pavement preservation* (NCHRP Report 680). National Cooperative Highway Research Program.

Yang, G., Li, Q. J., Zhan, Y. J., Wang, K. C. P., & Wang, C. (2018). Wavelet based macrotexture analysis for pavement friction prediction. *KSCE Journal of Civil Engineering*, 22, 117–124. https://doi.org/10.1007/s12205-017-1165-x

Zelelew, H., Khasawneh, M., & Abbas, A. (2014). Wavelet-based characterisation of asphalt pavement surface macro-texture. *Road Materials and Pavement Design*, *15*(3), 622–641. https://doi.org/10.1080/14680629.2014.908137

Zhao, G., Li, S., Jiang, Y., & Lee, J. (2018). *Quality assurance procedures for chip seal operations using macrotexture metrics* (Report No. FHWA/IN/JTRP2018/12). Purdue University, Joint Transportation Research Program.

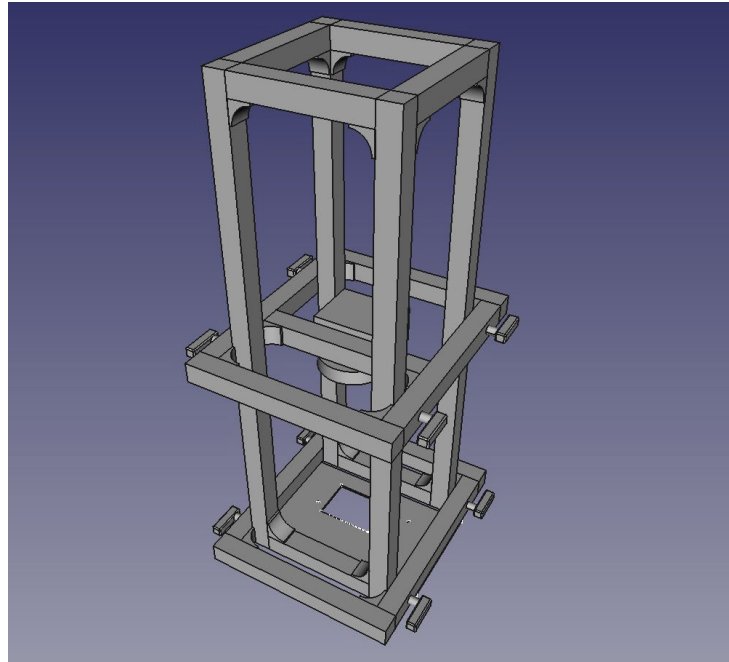# APPENDIX A: PROTOTYPE OVERHEAD IMAGE-TEXTURE FRAME

Figure 61. Schematic. A schematic of the overhead texture-image acquisition frame.
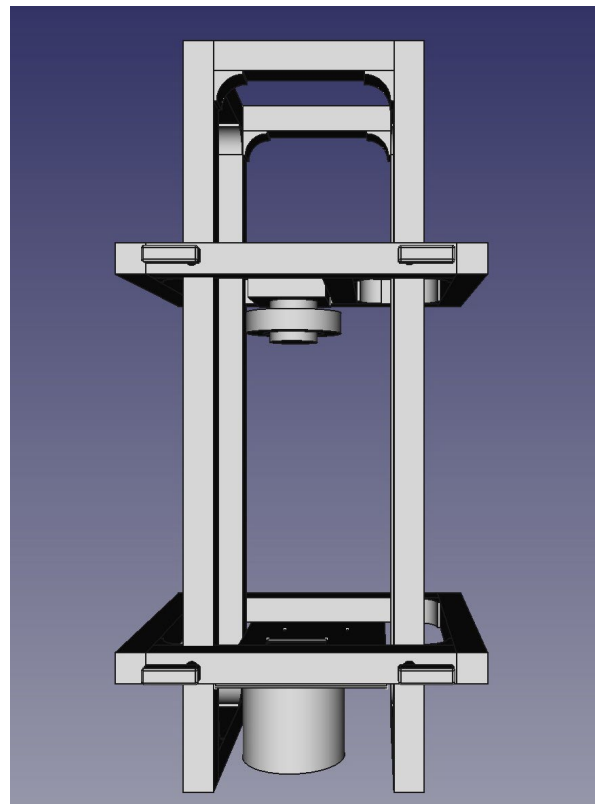

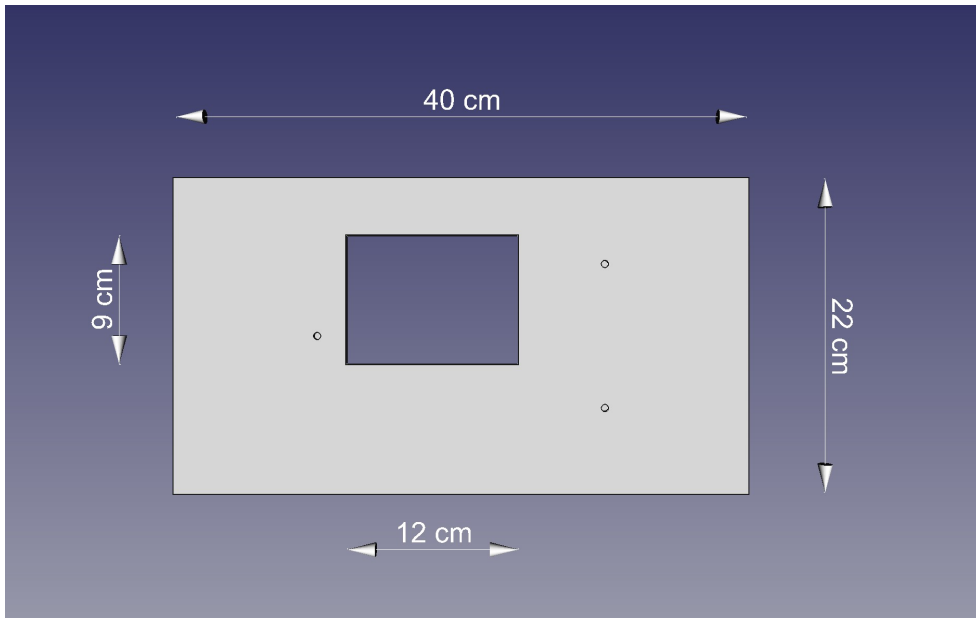**Figure 62. Schematic. Scanning frame with a core at the bottom.**

Figure 63. Schematic. Dimensions of scanning plate.
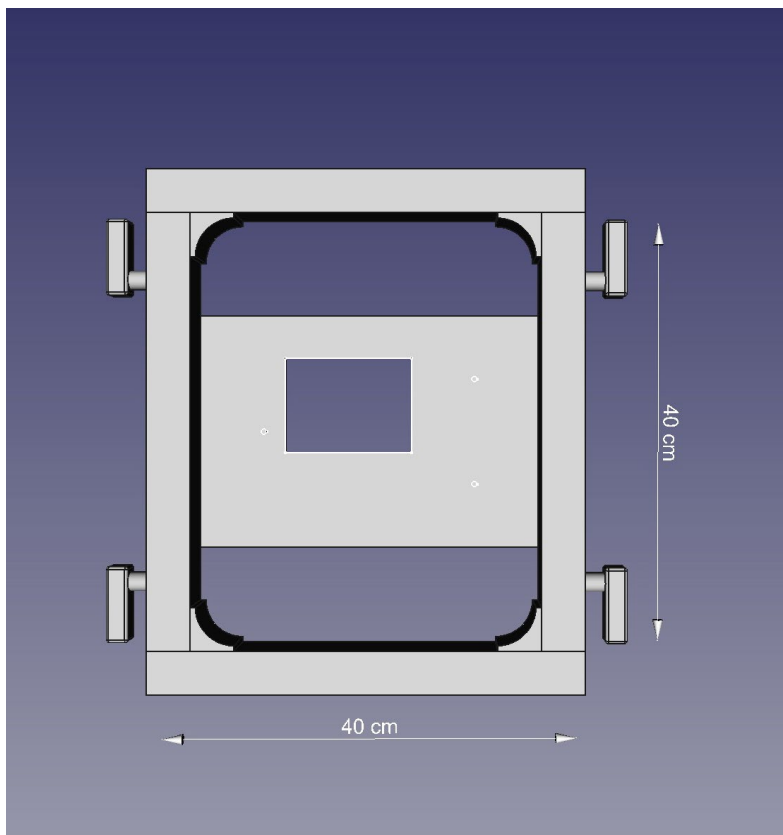

Figure 64. Schematic. Bottom scanning rack.

APPENDIX B: SIDE-VIEW IMAGE ANALYSIS

```
FOR EACH image in dataset:
    // Read image
    // Pre-processing
    Apply linear regression to correct angle of specimen surface
    Apply Gaussian blur to smooth the image and reduce noise

    // Convert image to HSV color space
    Convert image to HSV color space

    // HSV Thresholding
    Evaluate optimum HSV threshold range using developed tool
    FOR EACH pixel in image:
        IF pixel hue is within hue range AND pixel saturation is within saturation
        range
            AND pixel value is within value range:
            Set pixel as foreground (aggregate)
        ELSE:
            Set pixel as background

    // Post-processing
    Apply dilation to enhance aggregate regions
    Apply erosion to further refine aggregate regions
    Apply watershed algorithm to separate connected aggregates

    // Individual Aggregate Identification
    Numbering individual aggregates by numbering them based on coordinates

    // Top-layer Aggregate Selection
    Specify potential candidate of top-layer aggregates based on observation
    Exclude any aggregates that lay beneath others from potential list of
    aggregates (manual approach)

    // Main loop
    Create a new image to analysis using surface and list of top-layer aggregates
    Call the analysis function or decreasing/increasing binder level functions as
    needed
    Generate outputs (csv form) of detailed results containing whole values and
    its summarized results containing texture parameters and percent embedment
    calculation results


function calculate_msd(data):
    Apply low-pass filter to data
    Calculate average line value of data
    Divide data into left and right halves
    Find maximum value in left half (mx_l)
    Find maximum value in right half (mx_r)
    Calculate height in left half based on the average height, 'left'
    Calculate height in right half based on the average height, 'right'
```

```
        Calculate msd as the average of 'left' and 'right'
        Return msd

    function get_texture(img):
        Extract a top layer profile from the image
        Convert the profile to real-world measurements
        Calculate various texture parameters like mpd, ra, rms, rsk
        Create a dataframe with the calculated parameters
        Return the dataframe

    function segment_whitepx(white_px):
        Divide white pixels into chunks of consecutive pixels
        Keep only chunks with a certain minimum length
        Return the filtered list of chunks

    function segment_blackpx(black_px):
        Divide black pixels into chunks of consecutive pixels
        Keep only chunks with a certain minimum length
        Return the filtered list of chunks

    function get_avg_peak(arr): #Array of top-layer aggregates
        For each chunk in the input array:
            Calculate the maximum value in the chunk
            Add the maximum value to a list
        Calculate the average of the maximum values
        Return the average

    function identify_px(surface, img):
        For each node in the surface:
            Get neighboring pixels around the node
            Count black pixels among the neighbors
            If more than a threshold of black pixels, consider it an exposed area
        Return the arrays of black and white pixels

    function get_pe_peak_method(peak_agg, peak_binder, baseline):
        Calculate the PE using peak method formula
        Clip the result to the range [0, 1]
        Create a dataframe with the calculated values
        Return the dataframe

    function get_pe_circum_method(exposed_px, top_contours):
        Calculate the coverage ratio for each aggregate
        Calculate PE using circumference method formula
        Calculate lengths of exposed and all aggregate pixels
        Calculate mean of PE values
        Create a dataframe with the calculated values
        Return the dataframe

    function get_avg_height(segmented_px):
        Calculate average height from segmented pixels
        Return the average height

    function get_pe_avg_elev(h_a, h_b, baseline):
```

```
    Calculate PE using average elevation method formula
    Clip the result to the range [0, 1]
    Create a dataframe with the calculated values
    Return the dataframe


function decreasing_binderlv(img, step, iteration): #step: px number for iteration
    Create a copy of the input image and name it filled_copy # Binder only
    Initialize step and iteration variables
    Initialize x as 0
    Create a result directory for the current index idx
    Iterate while x is less than iteration:
        Iterate through each row i from the current top_point to (top_point + step):
            Iterate through each column j in the image:
                If the pixel at (i, j) is not white (255, 255, 255):
                    Set the pixel to white (255, 255, 255)
        Increment top_point by step
        Increment x by 1
        Draw AGG contours on the filled_copy image
        Get exposed pixels using get_exposedpx
        Perform texture analysis and other calculations
        Update the result dataframes
        Save images and dataframes to result directory


function increasing_binderlv(img, step, iteration): #step: px number for iteration
    Create a copy of the input image and name it filled_copy # Binder only
    Initialize step and iteration variables
    Initialize x as 0
    Create a result directory for the current index idx
    Iterate while x is less than iteration:
        Iterate through each row i from the current bot_point to (bot_point - step):
            Iterate through each column j in the image:
                If the pixel at (i, j) is white (255, 255, 255):
                    Set the pixel to black (0, 0, 0)
        Decrement bot_point by step
        Increment x by 1
        Draw AGG contours on the filled_copy image
        Get exposed pixels using get_exposedpx
        Perform texture analysis and other calculations
        Update the result dataframes
        Save images and dataframes to result directory
```

APPENDIX C: OVERHEAD TEXTURE-IMAGE ANALYSIS

```
load input image and convert to RGB format
load pre-trained Segment Anything Model (SAM) checkpoint
Configure mask generation parameters (points_per_side, pred_iou_thresh,
stability_score_thresh)
Generate masks using SAM model and input image

load segmented image
load cropped image
load LTS data and extract X, Y, Z values
2D Interpolate LTS data to match dimensions of cropped image

load segmented image and convert to grayscale
Identify contours in grayscale image using findContours

Sort contours by area in descending order

Select top percentage (e.g., 20%) of largest contours
for each selected contour:
    Create an empty binary mask of the same dimensions as the segmented image
    Draw the contour on the mask with white color to represent contour area

    Initialize empty lists: z_within_contour, z_all_coordinates

    for each LTS data point (X, Y, Z) within the contour:
        If (X, Y) falls within the contour area:
            Append Z value to z_within_contour

    Calculate average Z value for contour baseline by averaging z_within_contour

    for each pixel coordinate within the contour:
        Extract interpolated Z value from LTS data for the coordinate
        Append Z value to z_all_coordinates

    Calculate average Z value for the aggregate by averaging z_all_coordinates
    Calculate maximum Z value for the aggregate from z_all_coordinates

    find the coordinate with the maximum Z value within the contour
    Store the coordinate as highest_point_coordinate

    Store aggregate data:
        - List of coordinates within the contour
        - Average Z value for contour, baseline using boundary elevation
        - Average Z_all value for the aggregate, baseline using whole aggregate
          elevation
        - Maximum Z value for the aggregate
        - Coordinate the highest point

End loop
export result (coordinates, average Z, maximum Z values) for each aggregate
```